Marine Geology 274 (2010) 187–208

Contents lists available at ScienceDirect

Marine Geology

journal homepage: www.elsevier.com/locate/margeo

Highstand vs. lowstand turbidite system growth in the Makran active margin: Imprints of high-frequency external controls on sediment delivery mechanisms to deep water systems

J. Bourget [a,*], S. Zaragosi [a], S. Ellouz-Zimmermann [b], E. Ducassou [a], M.A. Prins [c], T. Garlan [d], V. Lanfumey [e], J.-L. Schneider [a], P. Rouillard [f], J. Giraudeau [a]

[a] Université de Bordeaux, UMR CNRS 5805 EPOC, Avenue des Facultés, F-33405 Talence, France
[b] IFP, Geology–Geochemistry–Geophysics, 1 & 4 avenue de Bois Préau, F-92852 Rueil-Malmaison, France
[c] VU University Amsterdam, Faculty of Earth and Life Sciences, De Boelelaan 1085, NL-1081 HV Amsterdam, The Netherlands
[d] SHOM, Centre Hydrographie, BP 426, F-29275 Brest, France
[e] IFREMER, GM/LES, BP70, F-29280 Plouzané Cedex, France
[f] UMR Géosciences Azur, Observatoire Océanologique—BP 48, F-06235 Villefranche-sur-Mer, France

ARTICLE INFO

Article history:
Received 18 December 2009
Received in revised form 13 April 2010
Accepted 15 April 2010
Available online 5 May 2010

Communicated by D.J.W. Piper

Keywords:
turbidite system
gravity flow
active margin
eustasy
climate
tectonics
earthquake recurrence
source-to-sink

ABSTRACT

Late Quaternary turbidite system growth along the Makran convergent margin is investigated through a set of deep-sea cores from upper slope and piggy-back basins to deep basin plain settings. High-resolution stratigraphy in these various depositional environments permits reconstruction of the evolution of sand-to-mud ratio, sedimentation rates, frequencies, and thickness of turbidite deposits during the last 25 ka BP. This study demonstrates how tectonics, climate and eustasy can interplay at high resolution (<20 ka) and control the input of terrigeneous sediment along the tectonically active Makran convergent margin, in a source-to-sink perspective.

The Makran turbidite system growth has been continuous throughout sea-level lowstand, transgressive, and highstand conditions. However, the frequency, rates, and nature of sediment supply varied in response to climate, sea-level, and tectonically induced changes in source-to-sink sediment dispersal modes. These changes include conditions of sediment production and availability in the drainage basin, capacity of transport from fluvial systems, and rates of sediment storage on the shelf and upperslope areas. Climate in the hinterland appears as a first-order control on the properties of turbidity currents that feed the turbidite system, controlling the average sand-to-mud ratio in the deep water deposits. The onset of sea-level highstand after ~8 ka BP resulted in a notable change in turbidite system growth, characterized by the occurrence of large volume, thick turbidity currents (>300 m thick along the continental slope) originated from successive, multiple slide or slump-induced surges. Their related deposits have low recurrence intervals, close to those calculated from the large magnitude earthquake and tsunami record in the Makran area.

Comparison with the Nile and Indus turbidite systems growth during the Late Quaternary provides an evaluation of the relative importance of shared forcing parameters (i.e. monsoon-induced phases of arid/humid conditions and post-glacial sea-level rise), in significantly different basin settings. The Indus fan appears mainly controlled by eustasy during the last 25 ka. Inversely, similarities are found between the Nile and Makran turbidite systems, where sea-level changes are modulated by the climate impact on fluvial dynamics in the hinterland. However, the Makran turbidite system growth is continuous through times, because both the uplift in the coastal area and the fluvial dynamics of short, mountainous river systems allow high sediment transfer rates to the marine basin, even though arid conditions and associated low water fluxes. Earthquake-induced highstand turbidite deposits form a thick sedimentary succession in the Oman abyssal plain, and are significant in the geologic record. This study finally illustrates how the complex interplay between external (allogenic) forcings can complicate the interpretation of high-resolution sedimentary successions in turbidite-filled basins.

1. Introduction

The nature and timing of sediment distribution in basins is mainly related to the dynamic processes and feedback mechanisms between

* Corresponding author. Present day address: Australian School of Petroleum, Reservoir Analogues Research Group, University of Adelaide, SA 5005 Adelaide, Australia. Tel.: +61 (0)8 8303 8023; fax: +61 (0)8 8303 4345.
E-mail address: j.bourget@asp.adelaide.edu.au (J. Bourget).

0025-3227/$ – see front matter © 2010 Elsevier B.V. All rights reserved.
doi:10.1016/j.margeo.2010.04.005

the external (allogenic) and internal (autogenic) forcings that govern sediment dispersal in erosional/depositional systems (Stow et al., 1985; Richards et al., 1998; Castelltort and Van Den Driessche, 2003; Allen, 2008; Sømme et al., 2009). As they represent the final position for source-to-sink sediment flux across continental margins, turbidite systems potentially record the interaction between climate, tectonic, and sea-level parameters, which strongly influence the timing, rates, and location of sediment supplied to basins. Impact of external forcings on sediment dispersal to the deep marine basins at short (<100 ka) time scales have been investigated for a long time, because they are important parameters governing the stratigraphic succession and resulting sedimentary architecture in deep water systems (Perlmutter and Mattews, 1989; Posamentier and Kolla, 2003). Although there has been some continued focus on sea-level in conceptual stratigraphic model that predict the delivery and formation of deep water deposits at 5th to 6th orders, corresponding to time scales <100 ka (Bouma et al., 1989; Posamentier and Vail, 1989; Posamentier et al., 1991; Brami et al., 2000; Catuneanu et al., 2009), an increasing number of studies show that climatically-driven variations in fluvial water and sediment discharge have a strong influence on turbidite system growth. This includes both glacially/ice-sheet-controlled (Skene and Piper, 2003; Zaragosi et al., 2006; Tripsanas et al., 2007; Toucanne et al., 2008); and monsoon-controlled (Ducassou et al., 2009) Pleistocene turbidite systems along passive margins. However, less data is available concerning high-frequency forcings on tectonically active systems such as fold-and-thrust belts depositional systems in convergent margins. Active margins are often associated with short river systems and fluvio-deltaic source, from which sediment supply is thought to be very sensitive to climate changes (Milliman and Syvitski, 1992; Weltje and De Boer, 1993; Mutti et al., 2003; Sømme et al., 2009). The importance of tectonics over global sea-level changes at long time scales have been observed in many tectonically active basins, uplift causing slope creation and forced-sea-level lowstands that promote changes in rates of sediment flux and depositional architecture (e.g. Mutti et al., 2003; Underwood et al., 2003). Earthquake-induced turbidite deposition along present-day active margins such as the Cascadia subduction zone, among others, show that tectonics can also influence the timing of sediment transfer to deep basins over short time scales (Goldfinger et al., 2007). However, the relative importance of short-term tectonic control on sedimentation in comparison to climate and eustasy remains poorly understood.

Our study investigates the growth pattern of the Makran turbidite system during the Late Quaternary from an extensive piston core data set that constrains high-resolution stratigraphy in various depositional environments (upper slope, piggy-back basins, canyon mouths and deep basin plain settings). Preliminary work done by Prins et al. (2000b), Prins and Postma (2000) and Stow et al. (2002) from a few cores in western piggy-back basins and abyssal plain suggested that turbidite deposition was frequent through the last sea-level lowstand (at ~20 ka), continued during the post-glacial rising sea-level and became infrequent after the onset of sea-level highstand (Prins et al., 2000b; Stow et al., 2002). However, detailed morpho-bathymetric analysis from a nearly complete subsurface mapping of the basin showed that the Makran turbidite system architecture and related sedimentary processes are highly variable along-strike (i.e. from east to west), depending of the upstream distribution of fluvial inputs and along-strike variation in tectonic regime (Bourget et al., in press). Thus, evolution of sediment input and turbidite system growth in the complex Makran setting cannot be only considered in isolated depositional environments, and must be analyzed at the system scale, both longitudinally and laterally. The Late Quaternary sedimentary infill of the Makran turbidite system is especially well-suited for investigating high-frequency interplay between climate, tectonics and eustasy as the margin is characterized by i) high convergence rates (~3 cm ka^{-1}; Ellouz-Zimmermann et al., 2007b) and significant uplift rates in the hinterland (Snead, 1967; Page et al., 1979; Vita-Finzi, 1987; Sanlaville et al., 1991; Hosseini-Barzi and Talbot, 2003); ii) strong terrigeneous sediment input from coastal streams and mountainous rivers (von Rad et al., 1999a; Luckge et al., 2001) and iii) high-frequency (<20 ka) monsoon-driven climate changes (i.e. arid/humid phases) in response to orbital and sub-orbital cycles during the last 25 ka (Sirocko et al., 1996; Schulz et al., 1998; Clemens et al., 2003).

Reconstructing the evolution of sand-to-mud ratio, sedimentation rates, frequencies, and thickness of turbidite deposits allowed a better understanding of how external forcings interplay at high resolution (<20 ka) and controlled the input of terrigeneous sediment along the tectonically active Makran convergent margin.

2. Regional setting

2.1. Tectonic setting and physiography

The Makran accretionary prism results from the northward subduction of the Arabian plate beneath the Iranian and Afghan continental blocks since the Late Cretaceous times (Kukowski et al., 2001; Grando and McClay, 2007; Ellouz-Zimmermann et al., 2007a; Fig. 1). The plate convergence rate has been estimated between 2.5 and 4 cm yr^{-1} (DeMets et al., 1994; Ellouz-Zimmermann et al., 2007b; Grando and McClay, 2007). The Makran subduction zone is an area of significant seismic activity (Quittmeyer, 1979; Ambraseys and Melville, 1982; Byrne et al., 1992; Ambraseys and Bilham, 2003), periodically affected by devastating earthquakes such as the 1945 Makran earthquake (M_w 8.1–8.3), which is the largest known in this region (Page et al., 1979; Ambraseys and Bilham, 2003; Bilham et al., 2007; Heidarzadeh et al., 2009). Low- to moderate-magnitude earthquakes (mainly related to thrust activity) occur more frequently (<50 y return time) in the Makran area (not restricted to the coast; Quittmeyer, 1979; Ambraseys and Bilham, 2003). The pattern of seismicity is distributed over a 700 km long and 200 km wide segment of plate boundary (Byrne et al., 1992; Ambraseys and Bilham, 2003). The Makran accretionary prism is more than 350 km wide (Platt et al., 1985). Over 60 % of the prism is presently sub-aerial, separated from the submarine part (~100–150 km) by a nearly undeformed continental shelf (Ellouz-Zimmermann et al., 2007a). This continental shelf is relatively narrow (from 10 to 40 km wide), with a shelf break at ~20 to 50 m water depth (Fig. 1). It only enlarges in the Sonmiani Bay area (Fig. 1), where it is about 100 km wide, with a shelf break at ca. −120 m (Fig. 1). The offshore (frontal) prism consists of a sequence of thrust slices units forming accretionary ridges (Fig. 1) with steep flanks and variable length, associated with intraslope "piggy-back" basins (White and Louden, 1983; Fruehn et al., 1997; Kukowski et al., 2001; Ellouz-Zimmermann et al., 2007b; Grando and McClay, 2007). The abyssal plain forms a smooth trench with low gradients, and is confined southward by the Murray Ridge (Fig. 1). To the west, it deepens and widens gently towards the Oman abyssal plain located at 3200 m water depth, where it becomes unconfined (Fig. 1). Sediments are brought to the basin by a dense network of streams and rivers distributed irregularly along-strike (i.e. from west to east). Numerous small ephemeral coastal streams are observed in the western Makran (Fig. 1), whereas larger, high-gradients rivers (such as the Hingol, the Pohr, or the Hab Rivers), which are more perennial, feed the eastern Makran (Fig. 1).

2.2. Past and present-day climate

The Arabian Sea corresponds to the present-day northern limit summer position of the Intertropical Convergence Zone (ITCZ; Gasse, 2000; Fleitmann et al., 2007). The present-day Makran climate is arid to semi-arid, but is dominated by the seasonal reversal of the

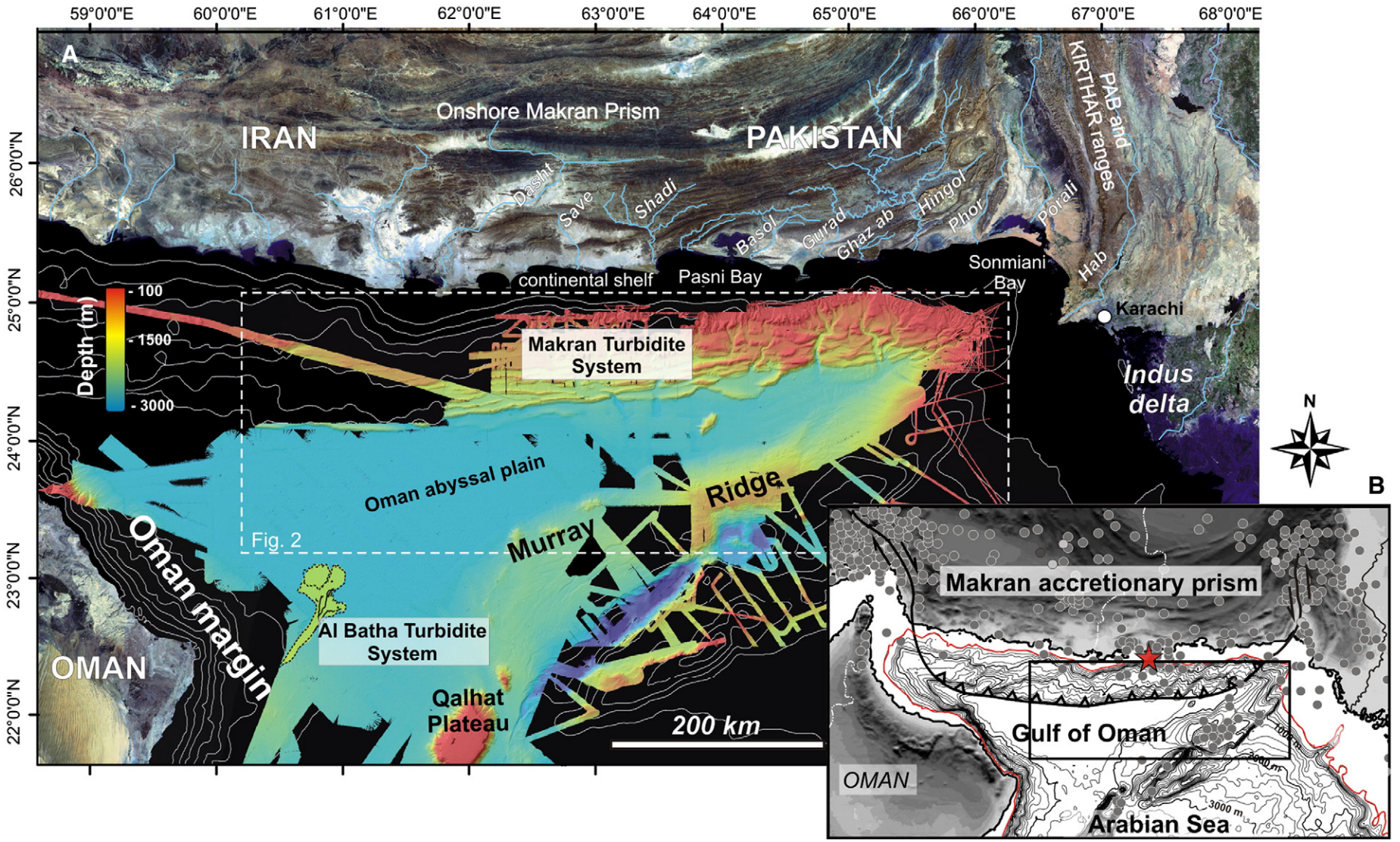

Fig. 1. (A) Location map and physiography of the study area. Location of the main rivers and streams. Bathymetry of the Gulf of Oman is issued from the compilation of MARABIE (2000, 2001) and CHAMAK (2004) surveys, combined with the existing hydrosweep data from SONNE 123 cruise (Flueh et al., 1997). (B) Tectonic setting and distribution of the recent earthquakes in the area (magnitude from 5 to 8/USGS database). The red star indicates the location of the 1945 earthquake epicentre (Byrne et al., 1992).

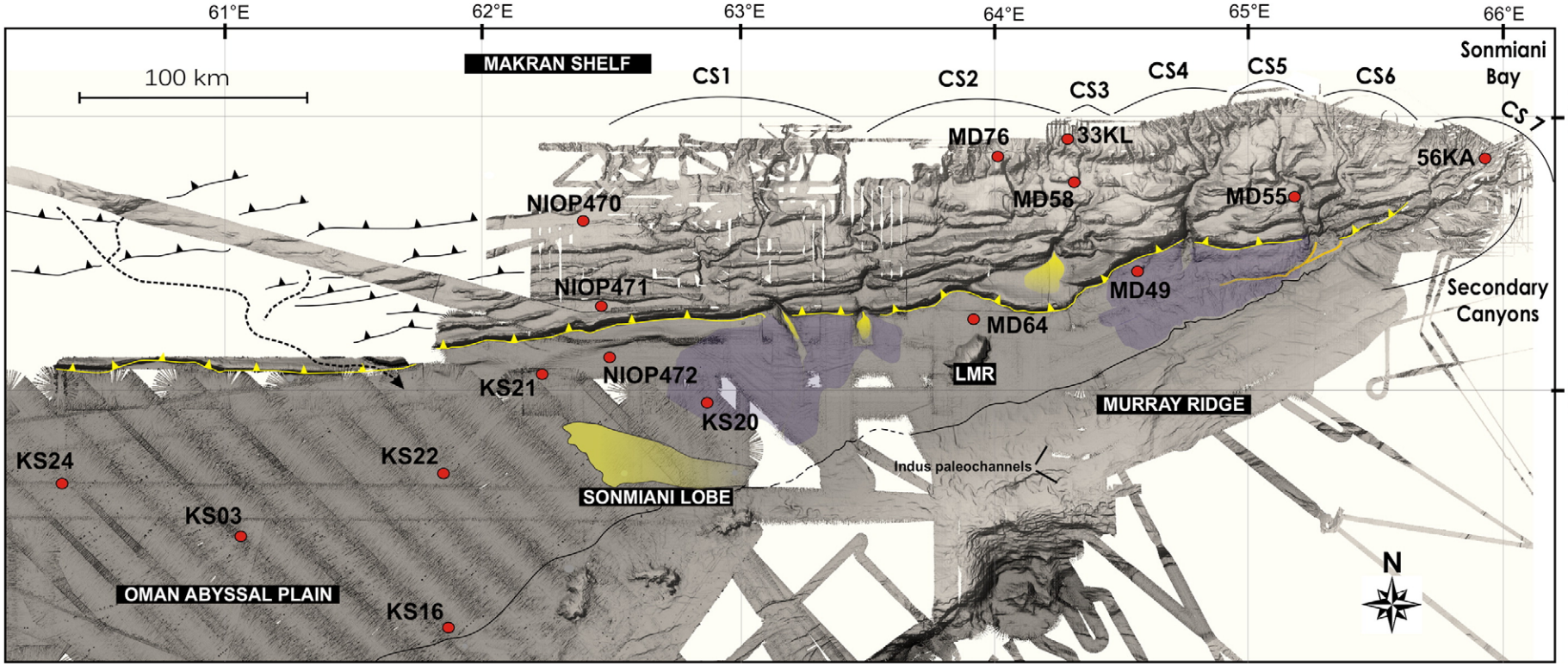

Fig. 2. Shaded bathymetry of the Makran turbidite system. Red dots indicate the location of sedimentary cores used in this study. Cores KS and MD55 (MD04-2855), MD58 (MD04-2858), MD49 (MD04-2849) and MD64 (MD045-2864) have been analyzed in this work. NIOP cores have been previously analyzed by Prins et al. (2000b) and Stow et al. (2002). Sedimentation rates and turbidite frequencies (when available) from cores MD76 (MD04-2876), 33 KL and 56 KA are obtained from published data of Böning and Bard (2009), and von Rad et al. (1999a, 2002b), respectively. CS = Canyon systems 1 to 7. Purple and yellow areas correspond to field sediment waves and main sand depocenters, respectively. LMR = Little Murray Ridge.

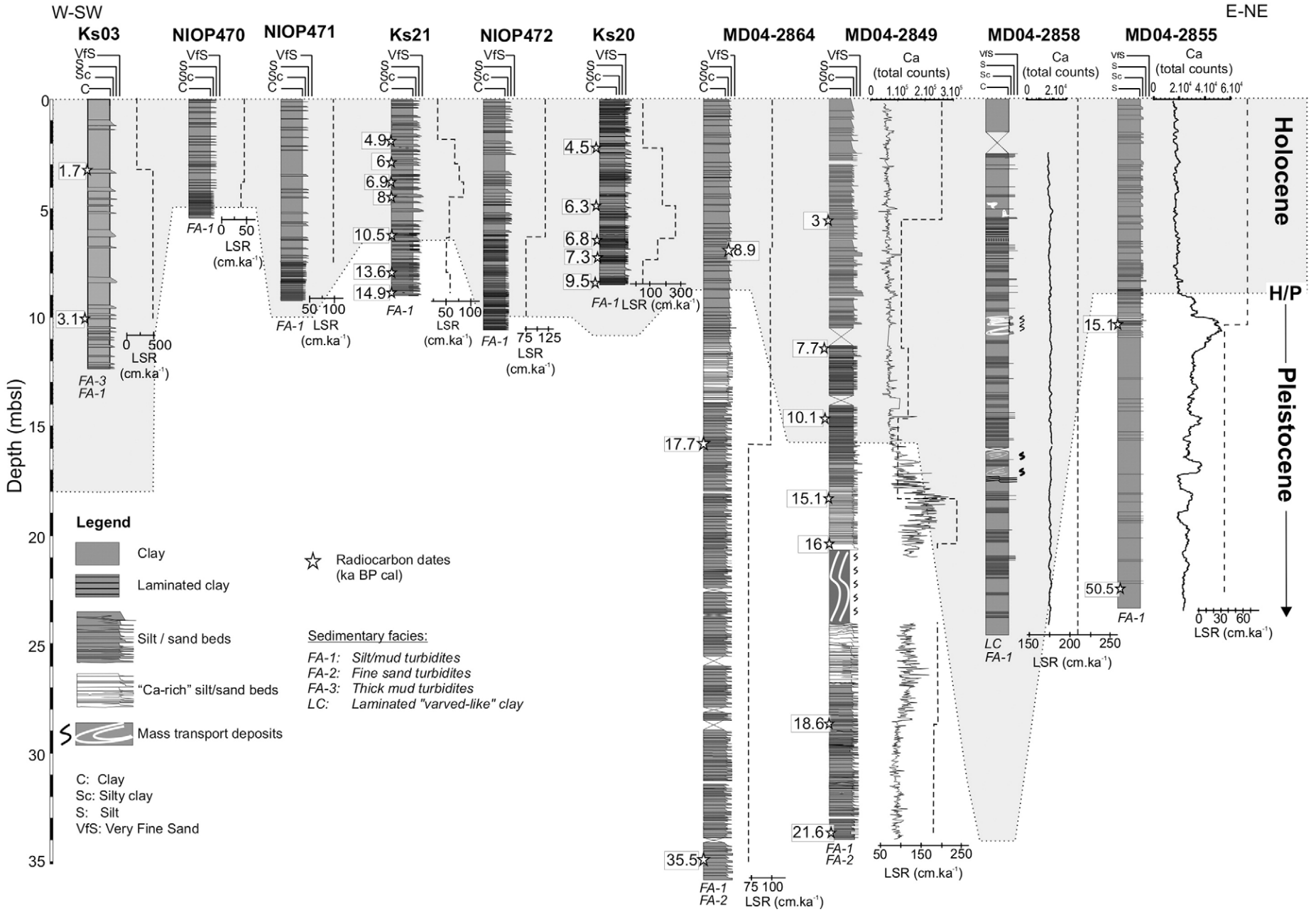

Fig. 3. Stratigraphy, sedimentary logs and facies occurrence, Ca content (XRF measurements), linear sedimentation rates (LSR, cm.ka^{-1}) and correlation of the sedimentary cores from the Makran continental slope and abyssal plain. Location of cores on Fig. 1. Stars indicate the calibrated AMS-14C dates (Table 2). Sedimentary facies (FA-1, FA-2, FA-3, and LC) refer to Bourget et al. (in press).

monsoon winds (Sirocko et al., 1991; von Rad et al., 1995; Luckge et al., 2001; Clemens and Prell, 2003). This leads to marked seasonal precipitations associated with a strong variability of water and sediment discharge at river mouths (von Rad et al., 1999a; Sirocko et al., 2000; Reichart et al., 2002). During the past, the Indian Ocean summer monsoon intensity has varied on Milankovitch (Clemens et al., 2003; Wang et al., 2003; Ruddiman, 2006; Clemens and Prell, 2007) and sub-Milankovitch (<15 ka) time scales (Sirocko et al., 1996; Schulz et al., 1998; Reichart et al., 2002; Leuschner and Sirocko, 2003; Wang et al., 2005). Numerous studies showed that the record of past summer monsoon intensity in the Arabian Sea points to striking similarities with the record of $\delta^{18}O$ from the Greenland GRIP and GISP2 ice cores, that documents rapid climate fluctuations during the last glacial–interglacial cycle (Sirocko et al., 1996; Schulz et al., 1998; Reichart et al., 2002; Leuschner and Sirocko, 2003). Productivity/aridity proxies from Arabian Sea cores evidenced that most recent periods of weak summer monsoon and enhanced aeolian transport were correlated to the northern hemisphere Last Glacial Maximum (~25 ka BP), the Heinrich event 1 (~19–15 ka BP), and the cool Younger Dryas (11.5–13 ka BP). Inversely, strong summer monsoon periods associated with increasing precipitations were inferred during the Bölling–Alleröd (from about 15 ka BP) and the early Holocene (after ~11 ka BP) interstadials (Sirocko et al., 1996; Schulz et al., 1998; Reichart et al., 2002; Leuschner and Sirocko, 2003; Pourmand et al., 2004). Particularly, the onset of the early Holocene humid period in the Gulf of Oman, and the return to more arid conditions after 5.5–7 ka BP is recorded in either marine sediments (Sirocko et al., 1996; Schulz et al., 1998; Reichart et al., 2002; Gupta et al., 2003; Pourmand et al., 2004; Ivanochko et al., 2005), stalagmites (Burns et al., 2003; Fleitmann et al., 2007), regional deserts (Glennie and Singhvi, 2002; Radies et al., 2004), and fluvial environments (Jain and Tandon, 2003; Juyal et al., 2006; Sridhar, 2007) of the surrounding area.

2.3. The Makran turbidite system

The Makran turbidite system (Fig. 2) is composed of a dense network of canyons, crossing high-relief accreted ridges and intra-slope piggy-back basins, that form connected and variably tortuous sediment pathways down a topographically complex slope (Kukowski et al., 2001; Bourget et al., in press; Mouchot et al., 2010). The upperslope sediments (until ~1800 m water depth) consist of laminated clays (Fig. 3) interpreted as "varved-like" sediments (von Rad et al., 1999a; Böning and Bard, 2009). It consists of annual couplets with "normal", hemipelagic sedimentation interbedded with terrigeneous layers related to suspension (plumite) deposits derived from short-term heavy rainfalls leading to flood events (von Rad et al., 1999a; Luckge et al., 2001 ; von Rad et al., 2002a; Bourget et al., in press). They are interbedded with mm-to-cm thick silt-mud turbidites (von Rad et al., 1999a; Bourget et al., in press). Satellite observation of a recent flooding event in the Makran coastal area shows that hypopycnal sediment-laden plumes can extend more than 40 km offshore (Fig. 4); i.e., beyond the shelf-break and the upper-slope, close to the coring sites 33KL (von Rad et al., 2002b), 56 KA (von Rad et al., 1999a) and MD04-2858 (Fig. 2). Middle and lower slope piggy-back basins are filled with hemipelagic deposits and/or gravity deposits, depending of their connection with the canyons (Prins et al., 2000b; Bourget et al., in press; Figs. 2 and 3). Downstream of the deformation front, the proximal trench is dominated by turbidite deposition (Bourget et al., in press; Fig. 3). Wide plunge pools associated with fine-grained turbidity current sediment waves (core KS20; Fig. 3) develop at the mouth of the western canyons (Fig. 2). The strong break of slope in these areas promotes erosional processes, sediment segregation, and only the finer-grained part of the gravity currents is transferred to the trench (Bourget et al., in press). Conversely, channel continuation is observed at the confluence of the eastern canyons (Fig. 2), allowing the transfer of

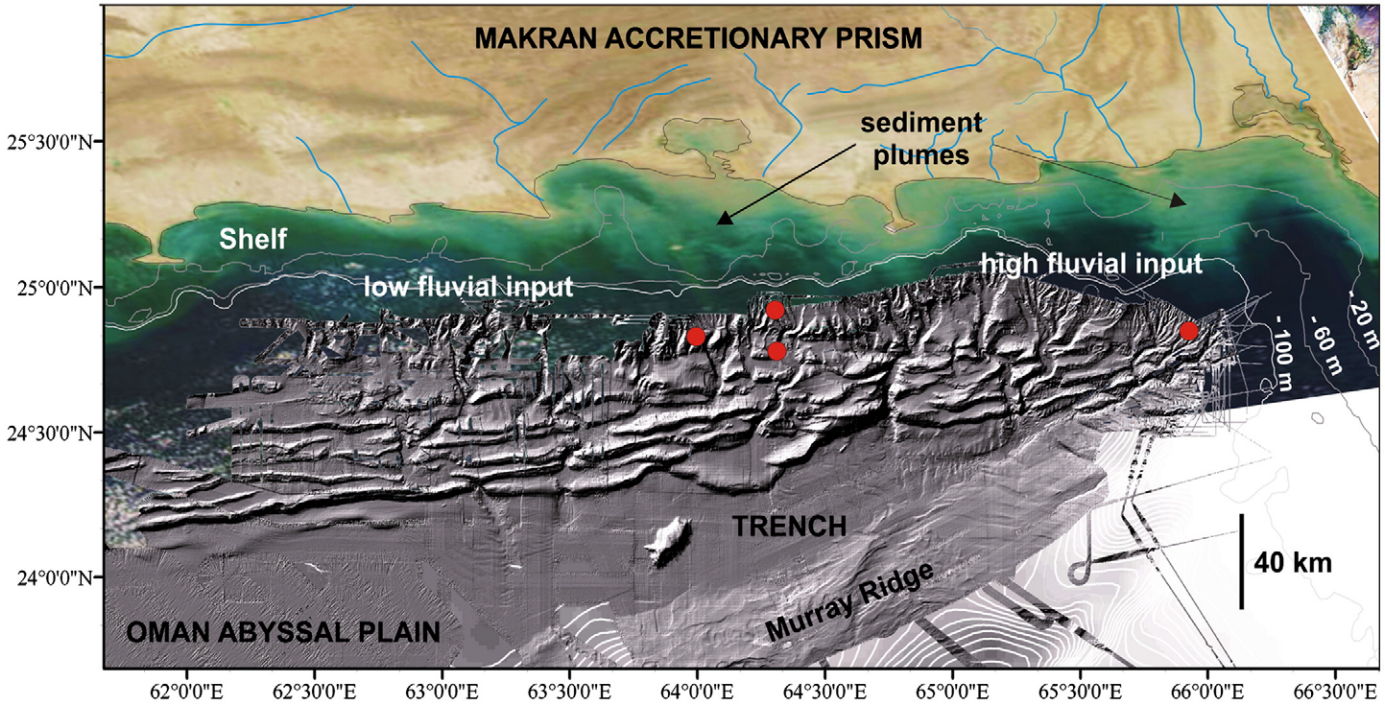

Fig. 4. (A) satellite (MODIS) image (1 km-resolution) taken during the winter 2005 flood event in the Makran coastal area (source: NASA Visible Earth—http://visibleearth.nasa.gov) showing the coalescing sediment plumes at the mouth of the Makran streams and rivers, and their seaward extension on the outer shelf and upperslope. This sedimentary dynamics is interpreted to be at the origin of the thick laminated clay Holocene sequence observed elsewhere in the upperslope cores (von Rad et al., 1999a; Luckge et al., 2001; von Rad et al., 2002b; Böning and Bard, 2009). These deposits, here observed in the core MD04-2858 (B), consist of flood-related ("plumites") terrigeneous laminae interbedded with hemipelagic (background), organic-matter rich laminae (e.g. von Rad et al., 1999a). Upperslope laminated sediments are usually stacked with silt-mud turbidites and mass transport deposits (MTDs) of local origin (C). Modified from Bourget et al. (in press).

Table 1
Key characteristics of the sedimentary cores analyzed in this study.

Core no.	Core location	Depositional environment	Depth (mbsl)	Length (m)
MD04-2858	65°10′48.459″E 24°42′13.138″N	Upper-slope piggy back basin	−1515	25.5
MD04-2855	64°19′42.429″E 24°44′55.814″N	Flank of Canyon 5	−1845	22
MD04-2849	64°33′14.469″E 24°25′39.251″N	Canyon 4 mouth	−3037	34
MD04-2864	63°55′0.230″E 24°15′34.479″N	Eastern abyssal plain (base of slope)	−3165	35
KS 20	62°52′19.891″E 23°57′27.367″N	Canyon 1 sediment waves	−3277	9
KS 21	62°12′55.214″E 24°3′55.589″N	Western abyssal plain (base of slope)	−3351	9.4
KS 24	60°19′53.120″E 23°39′51.969″N	Western abyssal plain	−3362	9.4
KS 22	61°49′46.596″E 23°42′38.771″N	Central abyssal plain	−3348	9.3
KS 03	61°7′50.982″E 23°32′36.149″N	Central abyssal plain	−3357	13.1
KS 16	61°50′46.970″E 23°9′13.222″N	Central abyssal plain	−3365	9.8
NIOP470	62°22′88.766″E 24°36′86.281″N	Mid-slope piggy back basin	−1840	5.5
NIOP471	62°27′50.550″E 24°18″39.714″N	Lower-slope piggy back basin	−2482	9.4
NIOP472	62°29′27.988″E 24°07′17.340″N	Western abyssal plain (base of slope)	−3274	10.4

coarser-grained material to the trench (Mouchot et al., 2010). The 3200 m deep, unchannelized Oman abyssal plain (Fig. 2) is composed by thick mud turbidites interpreted as basin-wide, sheet-like beds (Bourget et al., in press). The coarser-grained load of the flows entering the abyssal plain might be deposited at break of slope and in the ~1400 km^2 Sonmiani sandy lobe, which forms where the trench deepens and become unconfined (Fig. 2).

3. Materials and methods

This study is based on thirteen long piston cores recovered in the Gulf of Oman (Fig. 2). "KS" cores were acquired during the cruises MARABIE 2000 (*R/V Atalante*, IFREMER) and MARABIE 2001 (*R/V Le Suroît*, IFREMER), whereas "MD04" cores were acquired during the CHAMAK 2004 survey (*R/V Marion Dufresne II*, IFP/IPEV). "NIOP" cores were taken during the Netherlands Indian Ocean Programme by R/V Tyro (Prins et al., 2000b). The key characteristics of the cores analyzed in this study are displayed in Table 1. Facies description and interpretation have been previously presented and discussed by Bourget et al. (in press). The main sedimentary facies recognized in the cores are summarized in Fig. 3. Additional core data in the Makran upper slope (Fig. 2) comes from previous work by von Rad et al. (1999a) (core 56KA) and von Rad et al. (2002b) (core 33KL). Their previous results have been used to better constrain the nature and rate of Holocene sedimentation in the upperslope. Semi-quantitative geochemical element analyses were performed on most of the cores using X-ray fluorescence core scanners at cm to mm scale. Oxygen-isotope stratigraphy, based on the δ^{18}O analysis of the planktonic foraminifer *neogloboquadrina dutertrei* taken from the fraction 150–595 mm, was also constructed for core NIOP472 (Prins et al., 2000b). Core stratigraphy has been completed using several ^{14}C AMS dating from planktonic foraminifera species (Table 2). Radiocarbon dates have been corrected for a marine reservoir effect of 408 years and calibrated to calendar years using CALIB Rev 5.0/Marine04 data set (Stuiver et al., 1998) up to 21.78 ^{14}C ka and Bard (1998) thereafter. Radiocarbon ages of this study were performed at the 'Laboratoire de

Table 2
Radiocarbon ages of cores used in this study.

Core no.	Depth in core (cm)	Material	Uncorrected ^{14}C age (yr BP)	Calendar age (cal yr BP)
MD04-2849	550–560	Bulk pl. foram.	3215 ± 30	3027
MD04-2849	1142–1144	Bulk pl. foram.	7250 ± 30	7711
MD04-2849	1475–1476	Bulk pl. foram.	9270 ± 45	10,116
MD04-2849	1835–1836	Bulk pl. foram.	13,270 ± 60	15,191
MD04-2849	2032–2035	Bulk pl. foram.	13,870 ± 40	16,005
MD04-2849	2866–2867	Bulk pl. foram.	15,630 ± 60	18,644
MD04-2849	3376–3377	Bulk pl. foram.	18,580 ± 90	21,629
MD04-2855	1030–1031	Bulk pl. foram.	13,400 ± 60	15,146
MD04-2855	2241–2245	Bulk pl. foram.	47,700 ± 1200	50,252
MD04-2864	678–683	Bulk pl. foram.	8390 ± 35	8992
MD04-2864	1575–1577	Bulk pl. foram.	15,065 ± 45	17,759
MD04-2864	3497–3505	Bulk pl. foram.	31,480 ± 150	35,499
KS03	340–342	Bulk pl. foram.	2140 ± 30	1733
KS03	530–533	Bulk pl. foram.	3030 ± 30	2795[a]
KS03	1045–1047	Bulk pl. foram.	3290 ± 30	3136
KS16	315–316	Bulk pl. foram.	2390 ± 30	2020
KS20	217–218	Bulk pl. foram.	4465 ± 35	4656
KS20	482–483	Bulk pl. foram.	5865 ± 40	6283
KS20	660–661	Bulk pl. foram.	6415 ± 30	6896
KS20	717–718	Bulk pl. foram.	6775 ± 30	7304
KS20	871–872	Bulk pl. foram.	8295 ± 30	9573
KS21	197–199	Bulk pl. foram.	4730 ± 30	4958
KS21	278–279	Bulk pl. foram.	5630 ± 30	6029
KS21	355–356	*G. ruber* + *G. trilobus*	6445 ± 30	6933
KS21	460.5–461.5	Bulk pl. foram.	7605 ± 35	8065
KS21	618–619	Bulk pl. foram.	9715 ± 35	10,568
KS21	794.2–796	*N. dutertrei*	12,160 ± 60	13,613
KS21	880.5–882	*N. dutertrei*	13,065 ± 50	14,942

[a] Age is stratigraphically not consistent; data not incorporated in the age model.

Mesure du Carbone 14' in Saclay ('SacA') through the "ARTEMIS" radiocarbon dating project. All the ages in the following text are given in calendar age (cal ka BP). From "KS" and "MD04" cores, thin slabs (15 mm thick) were sampled and analyzed in the SCOPIX X-ray image processing tool (Migeon et al., 1999). Grain size analysis were performed using a Malvern™ Supersizer 'S'. This allowed a very detailed analysis of sedimentary structures and turbidite/hemipelagite/pelagite distinction. Turbidite thickness measurements were calculated from the turbidite base to the upper limit of the Te interval (Bouma, 1962). Turbidite thickness measurements from the NIOP cores only include the sand to silt, basal layer (Prins et al., 2000b).

4. Results

4.1. Stratigraphy and chronological framework

Core stratigraphy and age models have been achieved using a combination of twenty-six radiocarbon ages (Table 2), geochemical (XRF) data, and lithostratigraphy. NIOP cores have been correlated from the previous stratigraphic framework of Prins et al. (2000b) and Stow et al. (2002), based on lithostratigraphy (including grain size data), XRF data and stable oxygen isotopes. The sedimentological logs and the down-core distribution patterns of mean grain size and Ca content are shown in Fig. 3. Enhanced Ca values are recorded in discrete intervals in cores MD04-2849, MD04-2855, and NIOP-470, within radiocarbon ages that range between 16.4 ka BP and 14.9 ka BP. These intervals contain white to light grey turbidites showing higher XRF Ca values (Fig. 3). These sequences are also observed in the core MD04-2864, allowing lithostratigraphic core to core correlation (Bourget et al., in press; Fig. 3). Record of a Ca-peak in the Arabian Sea sediments at the end of the Last Glacial Maximum has been detailed by several authors (Reichart et al., 1998; Prins et al., 2000b; Klöcker and Henrich, 2006; Böning and Bard, 2009), and corresponds to a period of maximal NE monsoon intensity and continental aridity, synchronous to the North Atlantic Heinrich 1 event (Sirocko et al., 1996; von Rad et al., 1999b; Prins et al., 2000b; Pourmand et al., 2004; Böning and Bard, 2009). Values of Ca content weaken towards the Holocene/Pleistocene transition at ~11 ka BP (Klöcker and Henrich, 2006; Böning and Bard, 2009) and then remain low continuously through the Holocene (Fig. 3). In the core MD04-2849, a thick slump deposit (probably originated from the adjacent accreted ridge) is observed between 2072 and 2460 cm depth (Fig. 3). It can be considered as an "instantaneous" sedimentation, and has been deleted to the sediment record in the age model to correct the sedimentation rates.

4.2. Sedimentation rates

Linear sedimentation rates from the Makran cores are highly variable with time and core location (Fig. 3). Upper slope, river-derived sediments (core MD04-2858) are associated with very high sedimentation rates during the middle to late Holocene (about 214 cm ka^{-1}). This value is similar to the sedimentation rates of about 248 cm ka^{-1} found in core 33KL upslope (von Rad et al., 2002b), and 107 cm ka^{-1} in the core 56KA (von Rad et al., 1999a) for the last ~5 ka. In the middle and lower slope, significantly lower Holocene sedimentation rates are observed in turbidite-filled isolated piggy-back basins, disconnected from the main canyon systems (79–122 cm ka^{-1}; Fig. 3). Sedimentation rates in the right flank of the Canyon 5 (core MD04-2855) are low during the last glacial period (about 34.5 cm ka^{-1}) and then increase towards 68 cm ka^{-1} during the deglacial and the Holocene (from 15.1 ka BP; Fig. 3). In the trench, at the base of slope, turbidite sediments show mean Holocene sedimentation rates that range between 75 and 145 cm ka^{-1} (eastern prism; cores MD04-2849 and MD04-2864) to 58.5 and 91 cm ka^{-1} (in the western prism; cores KS20, KS21, NIOP472). In the deep Oman abyssal plain, thick mud turbidites caused high sedimentation rates ranging from 155 to 502 cm ka^{-1} for the last ~3 ka (Fig. 3).

4.3. Turbidite thickness and turbidite frequencies during the Holocene

Due to the variability of core length and location, only the last ~11 ka are fully recorded by the set of cores and allow correlation from the western to the eastern prism (Fig. 5). Turbidite activity has remained effective in the whole Makran turbidite system during the deglacial sea-level rise and Holocene highstand (Fig. 3). However, as previously observed by Prins et al. (2000b) and Stow et al. (2002), there is a marked change in the turbidite facies during the Holocene, dated at 8.1 ka BP and 8.3 ka BP in cores MD04-2849 and KS21, respectively, and estimated at 7.5 ^{14}C BP (about 7.9 ka BP cal) on the NIOP cores by Stow et al. (2002). It corresponds to a lower unit (~11–8 ka BP) of closely-spaced, thin-bedded turbidites, passing up to an upper unit (after ~8 ka BP) of thicker bedded but less abundant turbidites (Fig. 6). This change is clearly recognized in most of the cores recovered along the continental slope and trench (Fig. 5), and has been used as a lithostratigraphic marker to improve age models on the cores MD0428-55, MD0428-64, and NIOPs (Fig. 5). It should be noted that this turbidite thickness change is not recognized on the core KS20, located in a sediment waves fields at the mouth of Canyon 1 (Fig. 2). As it is distinctively observed in the adjacent NIOP-472 and KS21 cores (Fig. 5), we suggest that topographically induced autogenic processes such as local flow velocity increase and decrease or local confinement preclude a definitive allogenic facies change in this environment (Migeon et al., 2001; Ercilla et al., 2002).

Nonetheless, the evolution in turbidite system activity is highlighted by the evolution of turbidite frequencies through the Holocene on the whole dataset (Fig. 7). On each core, mean turbidite recurrence times have been estimated by counting the number of turbidites between the two chronostratigraphic intervals considered (i.e. between 0–8 ka and 8–11 ka). To avoid errors from age models, we used the closest absolute radiocarbon dates (Table 2), if available, rather than the 8 and 11 ka absolute positions calculated on the basis of linear interpolation. The age of the top of the cores was arbitrarily taken as 0 ka BP.

During the early Holocene (11–8 ka), turbidite recurrence times at the base of slope show mean values ranging from 31 to 77 years (i.e. 32 to 13 turb ka^{-1}; Fig. 7). Higher mean values of 226, 167, and 107 years are only observed in a more distal coring site (KS21), in an isolated piggy-back basin (NIOP-470), and on the flank of canyon 5 (MD04-2855), respectively (Fig. 7). In both slope and base-of-slope environments, these deposits correspond to mm to cm-thick, very fine-grained (silt to clay) and thinly bedded turbidites (Fig. 6).

After 8 ka and the onset of sea-level highstand, the calculated turbidite recurrence times increase in the whole basin and is homogeneous, considering the depositional environment of each coring site (Fig. 7): along the canyons axis, KS20 and MD04-2849 show mean recurrence times of 94 and 112 years, respectively (i.e. 11.5 and 9 turb ka^{-1}). Out of the canyon mouths areas (Fig. 7), recurrence times show similar values bracketed between 200 and 235 yrs (5–4.25 turb ka^{-1}). These turbidite frequencies are very close to those observed in the Late Holocene turbidite succession from the deep abyssal plain (mean recurrence time of 224 yrs, corresponding to 4.4 turb ka^{-1}, on the core KS03). Higher mean values (308–500 yrs; Fig. 7) are only observed in two western, isolated piggyback basins (cores NIOP470, NIOP471; Fig. 1). In both the continental slope and proximal trench cores (except KS20), these late Holocene deposits correspond to thicker (5–45 cm), very fine sand to silt basal, mud-rich turbidites (Fig. 6). The turbidite thickness increase distally, and form up to 180 cm thick sheet-like mud turbidites (Fig. 3).

Such low frequency turbidite activity after 8 ka contrasts with the synchronous sedimentation upslope (Fig. 7). Hence, in the Late

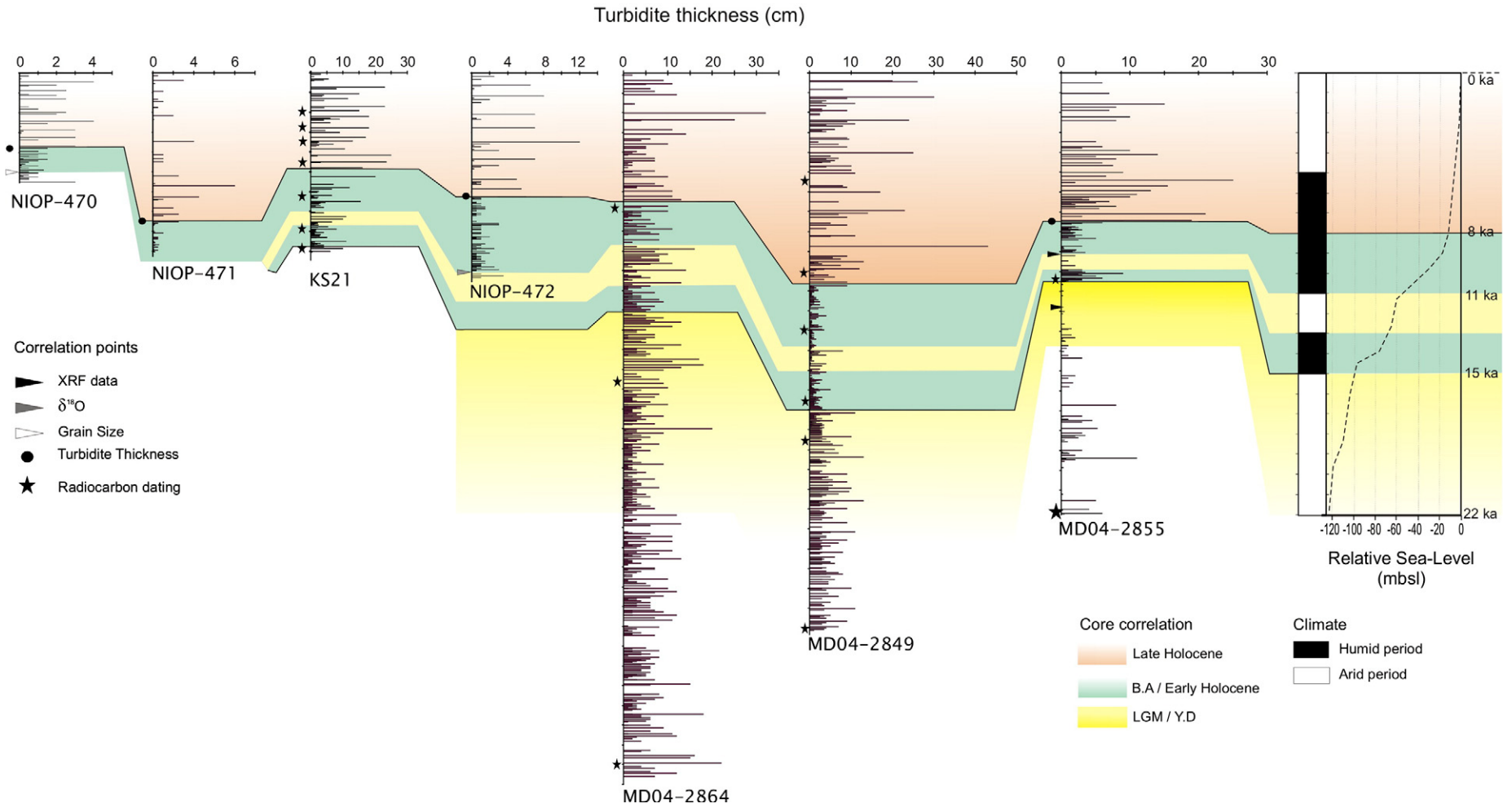

Fig. 5. Turbidite thickness (cm) measurements and stratigraphic correlation between the sedimentary cores from the Makran continental slope and abyssal plain. Lithostratigraphic, Ca content (XRF), grain size and δ18O data (from Prins et al., 2000b) are used as additional control points for stratigraphic correlation and age models. Relative sea-level curve is simplified from Fairbanks (1989) and Siddall et al. (2003).

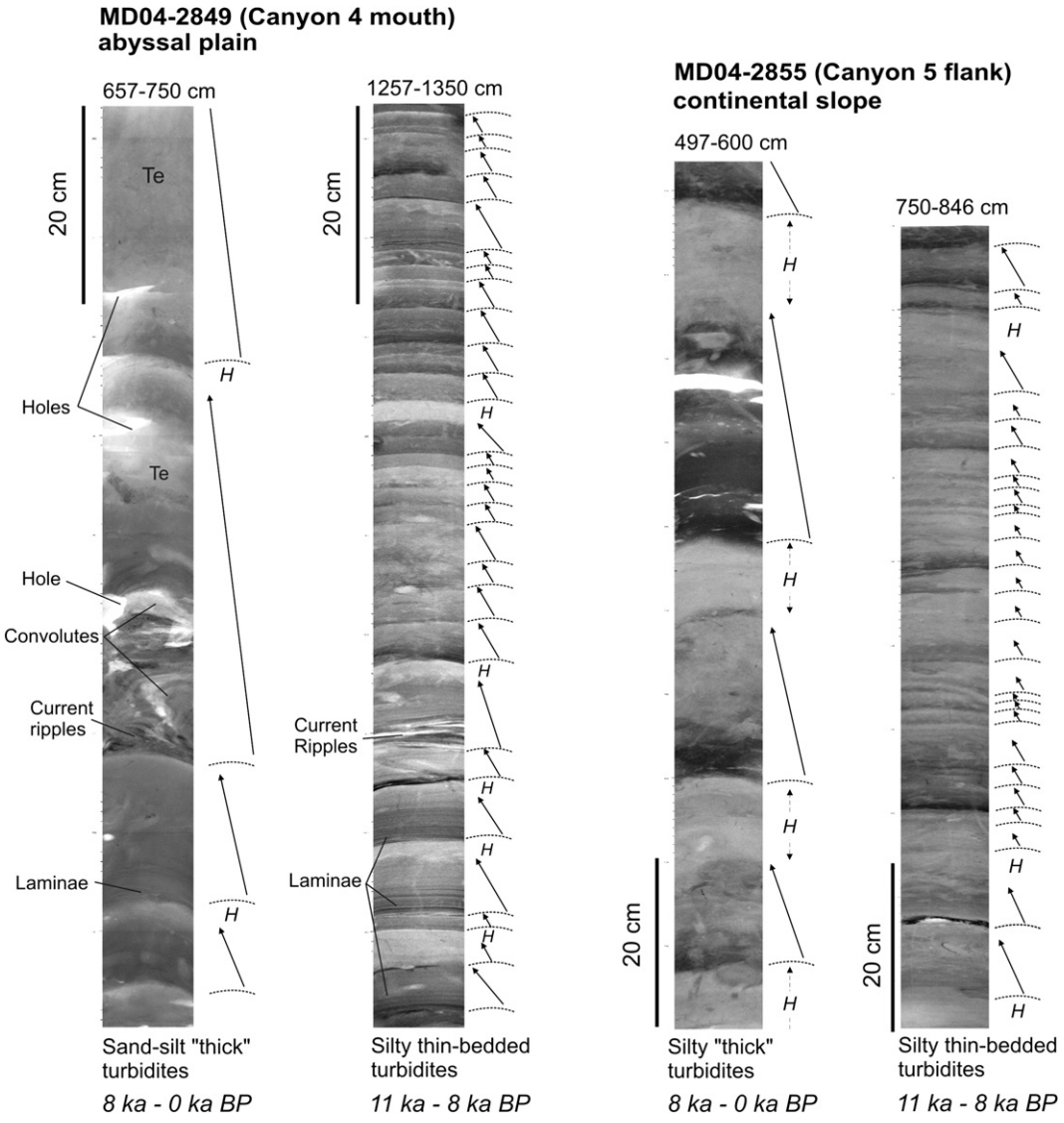

Fig. 6. X-ray pictures of selected sections from the cores MD04-2849 and MD04-2855, showing the variation in turbidite facies from the early Holocene (rising sea-level) and late Holocene (sea-level highstand) successions. H = hemipelagic/pelagic layers. Scale is similar on the four sections.

Holocene (last 5 ka) upper slope sediments, von Rad et al. (1999a) and von Rad et al. (2002b) calculated mean recurrence time of 14 and 17 years (Fig. 7) for flood-related events (i.e. thin silt/mud turbidites and detrital-rich "plume" deposits) in cores 33KL and 56KA, respectively (Fig. 1).

4.4. Sedimentary record since the LGM

Only a few cores provided a sedimentary record which covers the last ~25 ka BP (Fig. 3). We dated the base of MD04-2864 (abyssal plain) at 35.5 ka BP (Fig. 3). However, this core is located 110 km from the mouth of Canyon 4, and shows relatively low sedimentation rates and turbidite frequencies. It also lacks of grain size data and is poorly constrained by stratigraphic data. The core MD04-2855 covers the last ~50 ka BP, and is located at ~320 m above the canyon 5 floor (Fig. 3). Some core sections are only composed by hemipelagites, without turbidite deposits (Fig. 3). This suggests that this site only received the finest, upper part of thick, fully turbulent turbidity currents, which apparently only occurred during preferential periods (Fig. 5). Prior to the early Holocene, the most continuous sedimentary record is provided by the core MD04-2849 located close to the mouth of Canyon 4 (Fig. 3), which is the most developed canyon along the Makran continental slope. Hence, we used the cores MD04-2849 and MD04-2855 to evaluate the evolution of turbidite activity in the Makran turbidite system since the LGM. Four main periods have been differentiated from the turbidite record (Fig. 8):

a) from ~22 to 15 ka BP, mean sedimentation rates are about 166 cm ka^{-1} at the mouth of Canyon 4 (Fig. 8), with mean turbidite frequencies of ~20 turb ka^{-1} (corresponding to a time recurrence of 48 yr). Deposits during this time interval consist of thin-bedded (~10 cm), sandy turbidite (Fig. 8). In detail, turbidite activity slightly increases after 20 ka BP, and show a marked peak between 16 and 15 ka BP, associated with very high sedimentation rates (Fig. 8). However, this peak probably results from an artifact, as it is bracketed between two closely sampled AMS dates that could have enhanced a local bias in the age model. In MD04-2855, this period corresponds to very low turbidite sedimentation (2.3 turb ka^{-1}), indicating that either the thickness of the turbidity currents was mostly less than 320 m high during this time interval, or that there was a reduced turbidite activity along Canyon 5 (Fig. 8).
b) during sea-level rise, a mean turbidite activity of 33 turb ka^{-1} is observed on core MD04-2849 (corresponding to a time recurrence

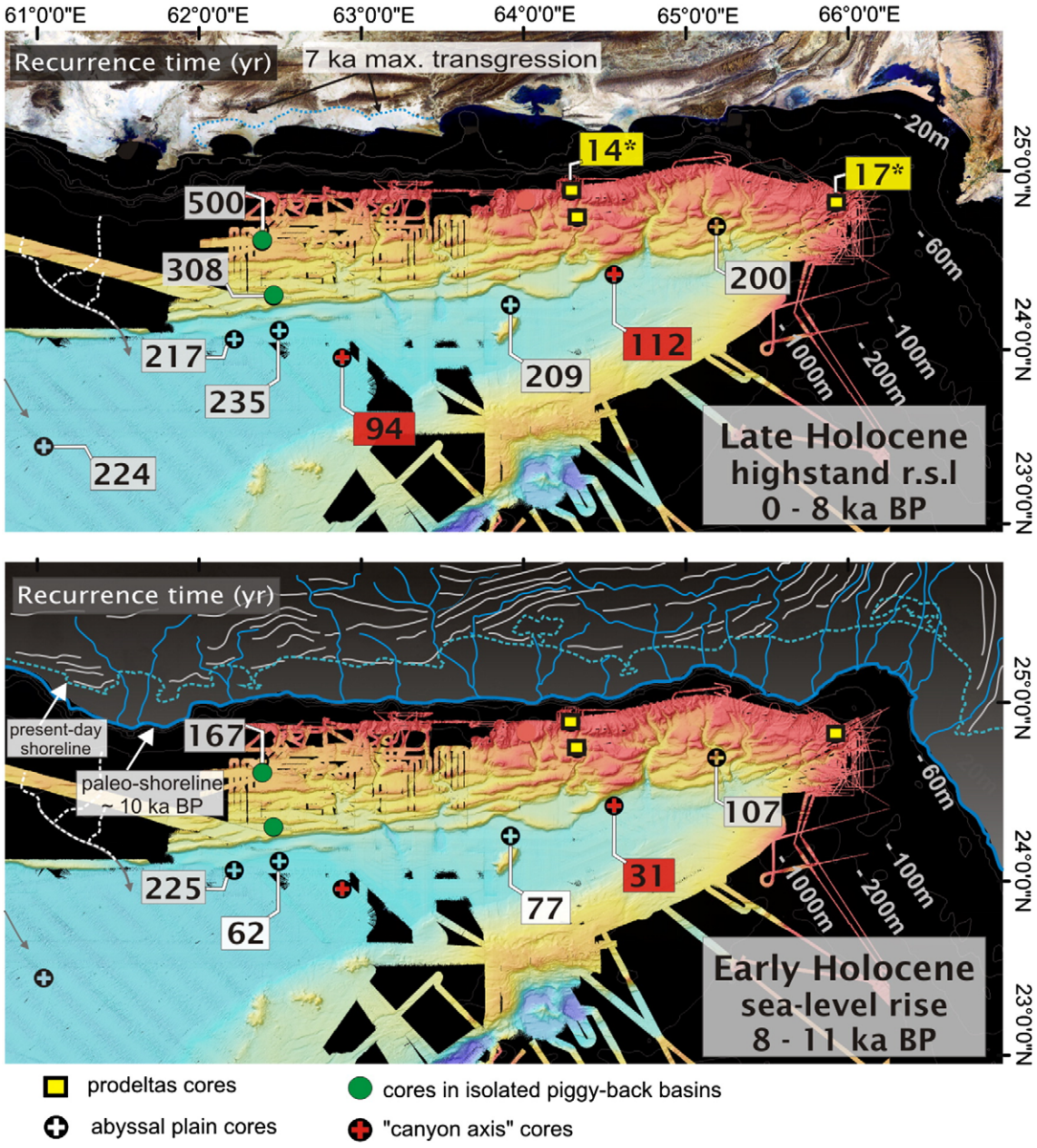

Fig. 7. Maps illustrating the distribution of turbidite time recurrence (years) during the early Holocene (coeval of sea-level rise and humid climate between 11–8 ka BP) and late Holocene (coeval of sea-level highstand and more arid conditions after ~8 ka BP). Recurrence times have been calculated from age models of the sedimentary cores. The approximate position of the paleo-shoreline at ~10 ka BP corresponds to a relative sea-level at −40 to −20 m below its present position (Fairbanks, 1989; Siddall et al., 2003). The position of the 7 ka BP paleo-shoreline corresponds to the maximum transgression identified by ^{14}C-dated paleo-beaches and lagoons, and plotted by Sanlaville et al. (1991).

of ~31 years). In detail, maximum frequencies at this location are observed at 15–13 ka BP and particularly at 12–8 ka BP, associated with very thin (<5 cm), generally very fine-grained turbidites (Fig. 8). Inversely, coarser-grained and slightly thicker beds are observed between ~13 and 11.5 ka BP, associated with a decrease in turbidite activity. On MD04-2855, turbidite sedimentation only occurs through the 15–13 ka BP and 11.5–8 ka BP peaks, the latter corresponding to increasing turbidite frequencies towards 9.3 turb ka^{-1} (Fig. 8).

c) in MD04-2849, turbidite frequencies abruptly decrease after 8 ka BP (towards 5.9 turb ka^{-1}; Fig. 8), while turbidite thickness increases and form thicker mud-rich turbidites with slightly coarser bases. These high turbidite sedimentation rates (103 cm ka^{-1}) during a sea-level highstand period are close to those observed during the lowstand interval (Fig. 8). Both sedimentation rates and turbidite frequencies slightly increase after 3 ka BP, reaching 176 cm ka^{-1} and 13.5 turb ka^{-1}. However, this could be an overestimation of the sediment thickness in the age model as we assigned the top of the core to "0 ka" arbitrarily. On MD04-2855, thick turbidite beds also occur after 8 ka (Fig. 8), while turbidite frequencies decrease (5 turb ka^{-1}), this interval corresponding to the maximum sedimentation rates (95 cm ka^{-1}) calculated on the 22 ka record at this site (Fig. 5).

5. Discussion

5.1. Makran turbidite system growth during the late Quaternary

Before considering the impact of changing sea level on the Makran turbidite system activity, we need to consider the importance of local tectonics on the local sea-level curve. Indeed, the Makran continental margin experiences a periodic uplift resulting from large-magnitude

earthquakes, evidenced along the coastal area by raised beaches and marine terraces. These features have been investigated by numerous authors in both the western and eastern prism (Snead, 1967; Page et al., 1979; Vita-Finzi, 1987; Sanlaville et al., 1991; Reyss et al., 1998; Hosseini-Barzi and Talbot, 2003). Raised Holocene accretion beaches, lagoonal deposits, and tombolos are found from the entrance of the Persian Gulf (to the west) to Karachi, in the Sonmiani bay (to the east). Their number and height increase to the east. The uplift

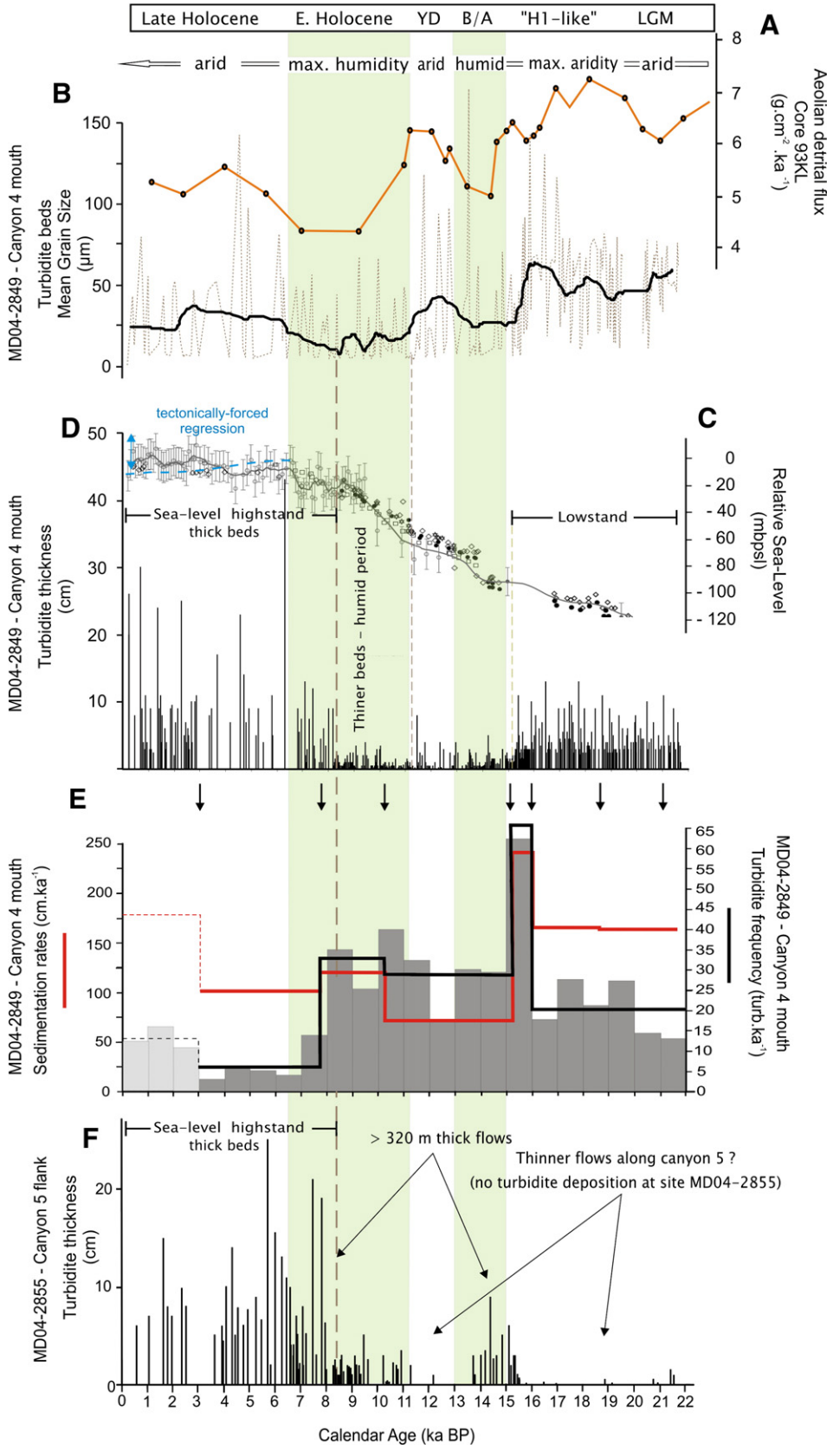

occurred continuously through the Pleistocene and Holocene as incremental steps, similar to the 1–3 m measured "instantaneous" uplift resulting from the 1945 Makran earthquake (Page et al., 1979). Uplift rates derived from ^{14}C dating of lagoonal and raised beaches fauna in many locations show that Late Pleistocene to Holocene uplift rates range from 0.1 to ~2 m ka^{-1} (Page et al., 1979; Vita-Finzi, 1987; Reyss et al., 1998; Hosseini-Barzi and Talbot, 2003). Considering the maximum value of 2 m ka^{-1} on the time span considered (last ~22 ka), we obtain a maximum uplift of 44 m. From 22 ka to 8–7 ka BP, the post-glacial sea-level rise of about 105 to 120 m has been achieved at rates of 7–8 m ka^{-1} (Fairbanks, 1989; Siddall et al., 2003), i.e. largely above the uplift rates. The relative sea-level reached its maximum transgression at about 7 ka BP in the Makran area, illustrated by uplifted paleo-beaches, lagoonal environments and archeology sites, now at 10–15 m above the present-day sea-level, and located 3 to 25 km north of the present-day coastline (Sanlaville et al., 1991; Fig. 7). This suggests that uplift significantly influenced Holocene progradation of the coastal Makran area, thus resulting in a small (10–15 m) tectonically forced regression (Posamentier et al., 1992) since the maximum transgression at 7 ka (Sanlaville et al., 1991). The latter is illustrated by paleo-beaches, lagoonal filling and fan-delta progradation along the coast (Sanlaville et al., 1991; Hosseini-Barzi and Talbot, 2003). Thus, although uplift impact could be considered as negligible during the deglacial period relative to the sea-level rise (uplift rates << transgression rates), it is significant after the Holocene sea-level stabilization.

From the sedimentary record observed in different depositional environments of the Makran margin, we can propose a first appraisal of the sedimentary system response from evolving climate and eustasy conditions during the Late Quaternary, in the context of active tectonics.

a) During the Last Glacial Maximum, sea level was about 105 to 120 m below its present position (Siddall et al., 2003), i.e. largely below the Makran shelf-edge that is located at −20/−50 m below present sea level (Fig. 9). The Makran rivers likely incised the narrow shelf and transported sediments directly into canyon heads or in the form of shallow-water, slope fan deltas (Fig. 9). Continental aridity and lack of vegetation during this period likely increased the production of coarse-grained sediments (Blum and Törnqvist, 2000). However, the relatively low LGM fluvial discharges might have enhanced aggradation of channels bends and sediment storage in ephemeral river systems, associated with aeolian sand deposition, which is a trend recorded in many fluvial systems from the drylands of north-western India, adjacent to the Makran coast (Jain and Tandon, 2003; Juyal et al., 2006). In the Makran turbidite system, sediment would have been discharged directly onto steep slope gradients either through hyperpycnal flows during occasional but catastrophic flooding, or from failures of shallow water sandy mouth bars and fan deltas accumulated at river mouths along a steep and unstable slope (Fig. 9). Gravity currents were frequent (~20 turb ka^{-1} at the mouth of canyon 4), producing cm to dm-thick sandy beds (Fig. 8). High availability of bulk material associated with the high proportion of bed-load transport by ephemeral, mountainous desert rivers during flood events (Laronne and Reid, 1993) likely favored the transfer of coarse-grained sediments by gravity flows with limited mud content, i.e. which could not develop a thick, fully turbulent nepheloid layer (Mulder and Alexander, 2001). This is suggested by the quasi-absent turbidite deposition on the flank of the Canyon 5 during the LGM (Fig. 8) indicating flows thinner than ~320 m thick (Fig. 9).

b) The post-glacial sea-level rise is synchronous with the transition from an arid period to humid conditions after ~15 ka BP (corresponding to the Bölling–Alleröd), and from ~11 to 5–7 ka BP (corresponding to the early Holocene humid period). At the mouth of Canyon 4, these periods are associated with thinner and finer-grained turbidite beds, but high sedimentation rates, as turbidite frequencies increased (Fig. 9). High turbidite frequencies are also recorded in most of the Makran depositional environments during the early Holocene humid period (Fig. 7), while very fine-grained, distal fluvial dispersions are observed in the Makran hemipelagic deposits (Prins et al., 2000b; Stow et al., 2002). Continental humidity enhanced higher water fluxes (i.e. more frequent floods of higher magnitude), but decreased the availability of coarse-grained material as a consequence of increasing vegetation cover (Blum and Törnqvist, 2000). The latter is evidenced by the evolution of pollen taxa in marine cores from the Makran continental slope (Ivory and Lézine, 2009). Post-glacial river incision, and transition from aeolian deposits and ephemeral river-beds to gravel braided or meandering fluvial systems, is observed in the adjacent semi-arid Indian region (Jain and Tandon, 2003; Juyal et al., 2006). Hence, the onset of maximum SW monsoon precipitations led to higher discharges, which likely generated erosion of channel beds and increase in sediment flux at the rivers outlets (Paola et al., 1992; Blum and Törnqvist, 2000; Van Den Berg Van Saparoea and Postma, 2008). Basinward, despite rising sea level and the progressive retreat of fluvial inputs, turbidity current frequencies increased in the trench and sedimentation rates remained high (Fig. 9). The abundance of very thin beds (<5 cm) deposited at high frequencies in both intraslope basins and trench suggests a frequent and regular sediment transfer to the deep basin during these humid phases. Hyperpycnal flows would have been an important turbidity current initiation process. Small-scale failures of mud-rich deltas rapidly prograding along the steep upperslope (e.g., Mulder et al., 1998) may also have supplied sediment to the Makran turbidite system (Fig. 9). Frequent failures of poorly consolidated and unstable material could have been easily triggered by rapid sediment loading, seismicity, or action of coastal hydrodynamics (i.e. wave erosion, rip-currents, and canyon head flushing; Piper and Normark, 2009). Evidence for turbidite deposition on the ~320 m high flank of Canyon 5 during the two humid intervals of 15–13 ka and after 11 ka BP is consistent with an interpretation of thick, mud-rich turbidity currents with a well developed, uppermost nepheloid layer (Mulder and Alexander, 2001).

The Bölling–Alleröd and early Holocene humid periods are separated by the more arid Younger Dryas phase bracketed between ~13 and 11.5 ka BP (Fig. 8). This period corresponds to an increase in

Fig. 8. Comparison between: (A) the evolution of the aeolian detrital flux (g cm^{-1} ka^{-2}) recorded from the Murray Ridge sedimentary record (core 93 KL; Pourmand et al., 2004). The increase in aeolian flux indicates enhanced conditions of winter monsoon strength, related to increasing conditions of aridity; (B) grain size data (D50, μm) from the turbidites bases of the core MD04-2849 (at the mouth of Canyon 4). Dotted line indicates the whole data, whereas the black solid line shows the five-points moving average grain size data; (C) Glacio-eustatic sea-level curve (in m below present sea-level) redrawn from Siddall et al. (2003), and adapted (for the last 7 ka; blue line) for the "forced-regression" calculated from the average uplift rates (see text for more details); (D) Turbidite-bed thickness (cm) evolution from the core MD04-2849 (including "Te"); (E) Linear sedimentation rates (cm ka^{-1}; red solid line), frequency of turbidite deposits (turb.ka^{-1}) calculated between two consecutive calibrated ^{14}C ages (black solid line) and using time slices (1 ka) of the age model (histograms) of core MD04-2849; Dashed lines and light grey histograms after 3 ka BP indicate the probable uncertainties of calculations as we used the top of the core as 0 ka BP (see text for more details); (F) Turbidite-bed thickness (cm) evolution from the core MD04-2855 (including "Te"), located at the top of the flank of Canyon 5. Location of sedimentary cores in Fig. 1. LGM corresponds to Last Glacial Maximum period; "H1-like" corresponds to the equivalent of the Northern hemisphere Heinrich event 1 (19–15 ka BP); B/A and YD correspond to the Bölling–Alleröd and Younger Dryas periods, respectively; E. Holocene corresponds to the early Holocene period (11 to 7–5,5 ka BP).

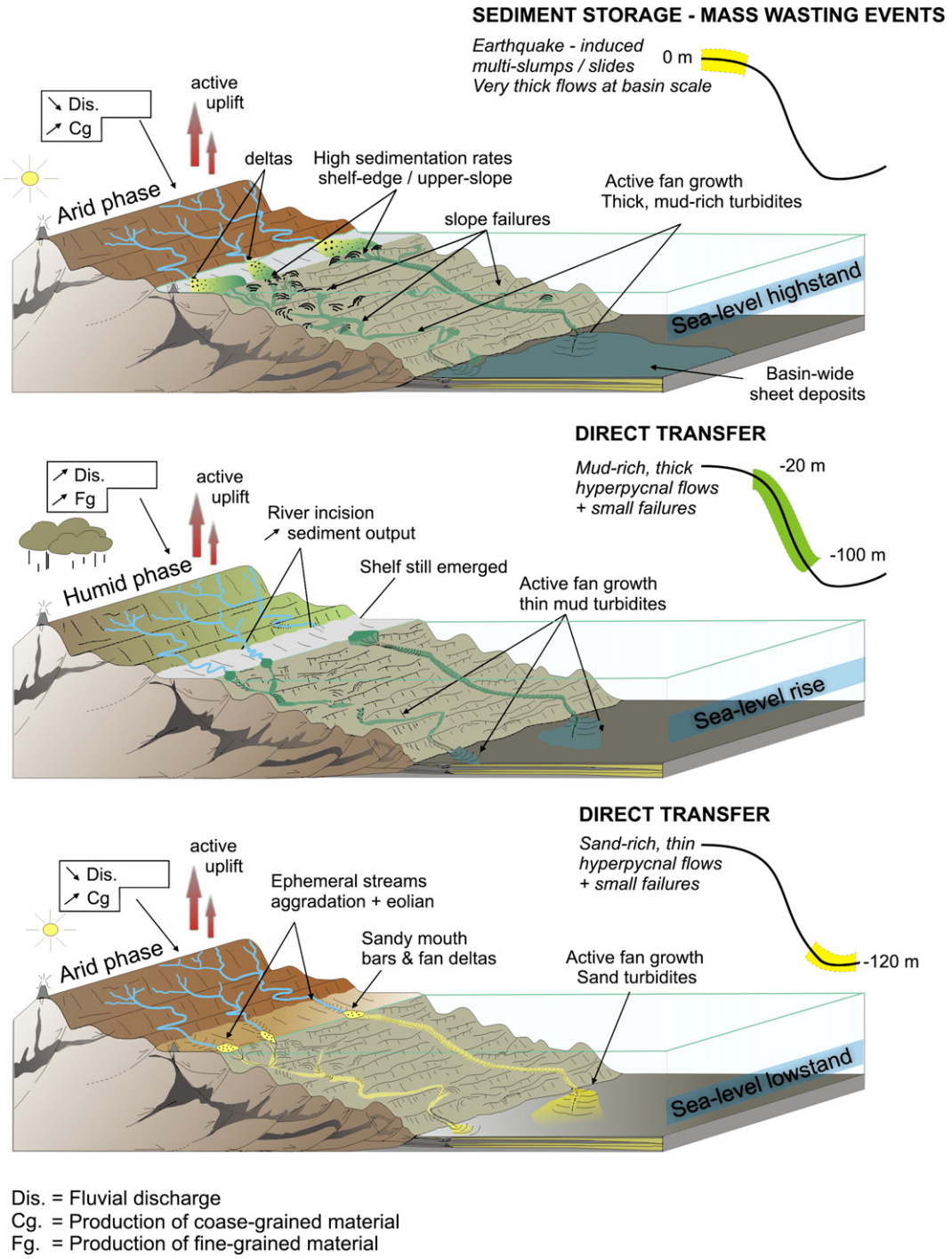

Fig. 9. Conceptual model for Makran turbidite system growth and evolution of source-to-sink sedimentary processes during the late Quaternary, in relation with climate, eustasy, and tectonics. Relative sea-level curve is simplified from Fairbanks (1989) and Siddall et al. (2003).

grain size of turbidite beds associated with a slight decrease in turbidite frequencies and sedimentation rates on core MD04-2849 (Fig. 8), synchronous with a nearly-absent turbidite record on core MD04-2855 (Fig. 8). Although more data is needed to extend observations in the whole margin, this could suggest a rapid basin response to high-frequency climate change, with enhanced production of coarser particles episodically transferred to the turbidite system by sand-rich, thin turbidity currents, i.e. a return to conditions more similar to the LGM (Fig. 8).

c) Despite persistent humid conditions until 6 to 5 ka BP (Fleitmann et al., 2007), the activity of the Makran turbidite system unequivocally shows a marked change at around 8 ka BP, i.e. when the sea-level fully inundated the narrow continental shelf (Fig. 9). Turbidite frequencies show a rapid and important decrease in both piggy-back basins and abyssal plain (Fig. 7). However, the increase in thickness of each individual turbidite bed enhance exceptionally high turbidite sedimentation rates for a sea-level highstand period, quite similar than those observed during lowstand and rising sea-level periods (Fig. 3). Occurrence of thicker turbidite beds in the Makran continental slope and abyssal plain indicate that the basin is fed by rare, larger volume, mud-rich turbidity currents. Significant turbidite deposition on core MD04-2855 also indicates that such turbidity currents were more than 320 m high along

Canyon 5 (Fig. 8). Rapid margin progradation and tectonically induced regression during this period likely promoted high rates of sediment transfer to the Makran shelf and slope (von Rad et al., 1999a; von Rad et al., 2002b). Very high sedimentation rates and flood-related beds are observed in the upperslope sediments (Fig. 7), suggesting that the large amounts of bulk material supplied by the Makran rivers during flood events are mostly stored on the shelf and upper slope in sea-level highstand conditions (Fig. 9). Failures along the upperslope could lead to occasional flushing of sediments to the basin plain (Fig. 9), generation of large-volume turbidity currents, and thus growing of the Makran turbidite system even during sea-level highstand conditions. Such failures are likely triggered by overloading and escape of pore fluids in high accumulation rates sediments, storm waves loading during the summer monsoon seasons, or related to earthquake events. The latter point will be discussed hereafter.

The late Holocene regional climate is marked by a shift towards more arid conditions after ~5 ka BP, associated with a change in regional hydrologic regimes with an important decrease in discharge, width/depth ratio, and a return to more ephemeral, sand-bed streams (Jain and Tandon, 2003; Sridhar, 2007). Decrease in vegetation is associated with enhanced production of bulk material in the drainage basins (Blum and Törnqvist, 2000), which could be highlighted by the increase in mean grain size of turbidite beds at the mouth of Canyon 4 (Fig. 8), in comparison to the humid periods. This could also be related to higher peak flood discharges and transport competence in the rivers during arid conditions (Laronne and Reid, 1993). The east to west (along-strike) distribution of the Makran rivers in the present-day setting allows a quasi-continuous delta-mouth and prodelta sedimentation along the continental shelf, that could be at the origin of the very dense and continuous canyon and gullies network in the present-day upperslope, that converge into larger systems downslope (Fig. 2).

5.2. Implications for the subduction earthquake and tsunami record in the Arabian Sea

Average earthquake recurrence time deduced from turbidite records have been performed in several active margin setting including the Cascadia subduction zone (Goldfinger et al., 2007) and the South-Chilean margin (Blumberg et al., 2008). The record of large reworking events such as earthquake-induced turbidity currents requires a sufficient volume of sediment accumulated upslope, and thus a minimum residence time in a staging area. In most cases, canyons have been disconnected from the rivers during the Quaternary highstand periods of sea level. As observed in the Makran turbidite system, sea-level highstand conditions reduce the possibilities to rapidly transfer the sediments from continent to deep-water (i.e. by hyperpycnal flows, mouth-bar failures, rip-current erosion or storm wave erosion), while sediment storage capacities on the shelf and upperslope increases. In areas where climate does not dramatically reduce continental erosion and sediment transfer basinward, such as observed in glacially influenced areas like the Chilean forearc (Blumberg et al., 2008), the Holocene sea-level highstand period can thus could be better adapted to record earthquake-induced gravity flows.

However, there are still several possible triggering mechanisms for turbidity current generation during highstand periods, and numerous investigators have attempted to distinguish seismically generated turbidites from flood, storm-induced, or other marine gravity deposits (Mutti et al., 1984; Nakajima and Kanai, 2000; Shiki et al., 2000). Our results show that the Late Holocene turbidite sedimentation in the frontal Makran accretionary prism and trench consists of large-volume turbidity currents probably initiated by failures of slope sediments (Fig. 9). In the Oman abyssal plain, late Holocene deposits consist of thick, sheet (basin-wide) muddy turbidites (Fig. 10), for which the minimum estimated volume exceed 4 km^3 for a single event (Bourget et al., in press). These thick turbidite deposits are commonly characterized by a well developed (up to 150 cm) uppermost clayey (Te) layer (resulting from the slow decantation of a thick nepheloid cloud), as well as a complex internal structure and silt-bed recurrence. These deposits have been interpreted as the product of slump- or slide-triggered, large volume and mud-rich turbidity currents (Bourget et al., in press), in which velocity, shear mixing rate or volume of failed sediment in motion vary through time (Wynn et al., 2002; Talling et al., 2007). The overall complex internal structure also suggests that such flows occur as successive surges forming a single, thick turbidity current (Lowe, 1982; Kneller, 1995; Wynn et al., 2002; Tripsanas et al., 2004).

Similarly, several authors interpreted turbidites with wide areal extent, complex internal structures with multiple coarse fraction pulses, and variable provenance (derived from multiple or line sources), as the product of a series of surge-type flows derived from seismically triggered, multiple slumps/slides on slopes (Mutti et al., 1984; Nakajima and Kanai, 2000; Shiki et al., 2000; Goldfinger et al., 2003). Numerous slides took place along the continental slope during the 1929 Grand Banks earthquake (Piper et al., 1988), and produced several independent turbidity surges that flowed down different valleys and formed an amalgamated deposit on the Sohm abyssal plain (Piper and Normark, 2009). Similarly, during the 1945 Makran earthquake event, submarine cables were broken at eight different places by several submarine slides and/or gravity currents (Ambraseys and Melville, 1982; Bilham et al., 2007). Thus, we assume that transformation of co-seismic slump and/or slides are at the origin of the thicker turbidite beds deposited since ~8 ka in the whole Makran turbidite system. This produces distally coalescing flows which generate the very thick, sheet-like mud turbidites draping the Oman abyssal plain (Fig. 10). Co-genetic mass wasting events could episodically rework large volumes of shelf-edge and upper slope muds. Continental uplift and flash flooding promotes very high sediment flux and sedimentation rates in these fine-grained deposits. This could have hindered the escape of pore fluids, thus favouring slope failure (Garziglia et al., 2008). Additional sediments could be flushed into the canyons through mass wasting along the steep canyon walls, as suggested by the present-day bathymetry (Bourget et al., in press). Significant amount of material by downslope erosion from ignitive turbidity currents (Parker, 1982; Piper and Aksu, 1987) along the steep submarine canyons (Bourget et al., in press) could finally account for the total volume of sediment deposited downslope. Sedimentological evidence of multiple-sourced, large volume flows, could thus be considered as a proxy for slump/slide-induced gravity currents, eventually (but none exclusively) triggered by large magnitude earthquakes.

In the Makran turbidite system, average recurrence time for these highstand deposits show values of ~100 years in the canyons axis, and 200–235 years in more distal positions (Fig. 7). Historical seismicity is poorly constrained in the Makran area due to the sparse population and the lack of technical records. However, regional earthquake catalogs suggest that large magnitude earthquakes such as the 1945 event occur at recurrence time of about 125–250 years along the eastern Makran coastal and submarine areas (i.e. from the Iranian–Pakistani border to Karachi; Page et al., 1979; Ambraseys and Melville, 1982; Byrne et al., 1992; Ambraseys and Bilham, 2003; Heidarzadeh et al., 2009). Taking account of the uncertainties and error intervals of both earthquake record and turbidite dating, the recurrence time of the late Holocene Makran turbidites appear well correlated with the large-earthquakes recurrence upslope. Storm-induced surges or lower-magnitude earthquakes would eventually form single flows producing deposits of smaller extent, and resulting to slightly higher turbidite frequencies near the canyon mouths (Fig. 7). They could also result from low-frequency, high magnitude

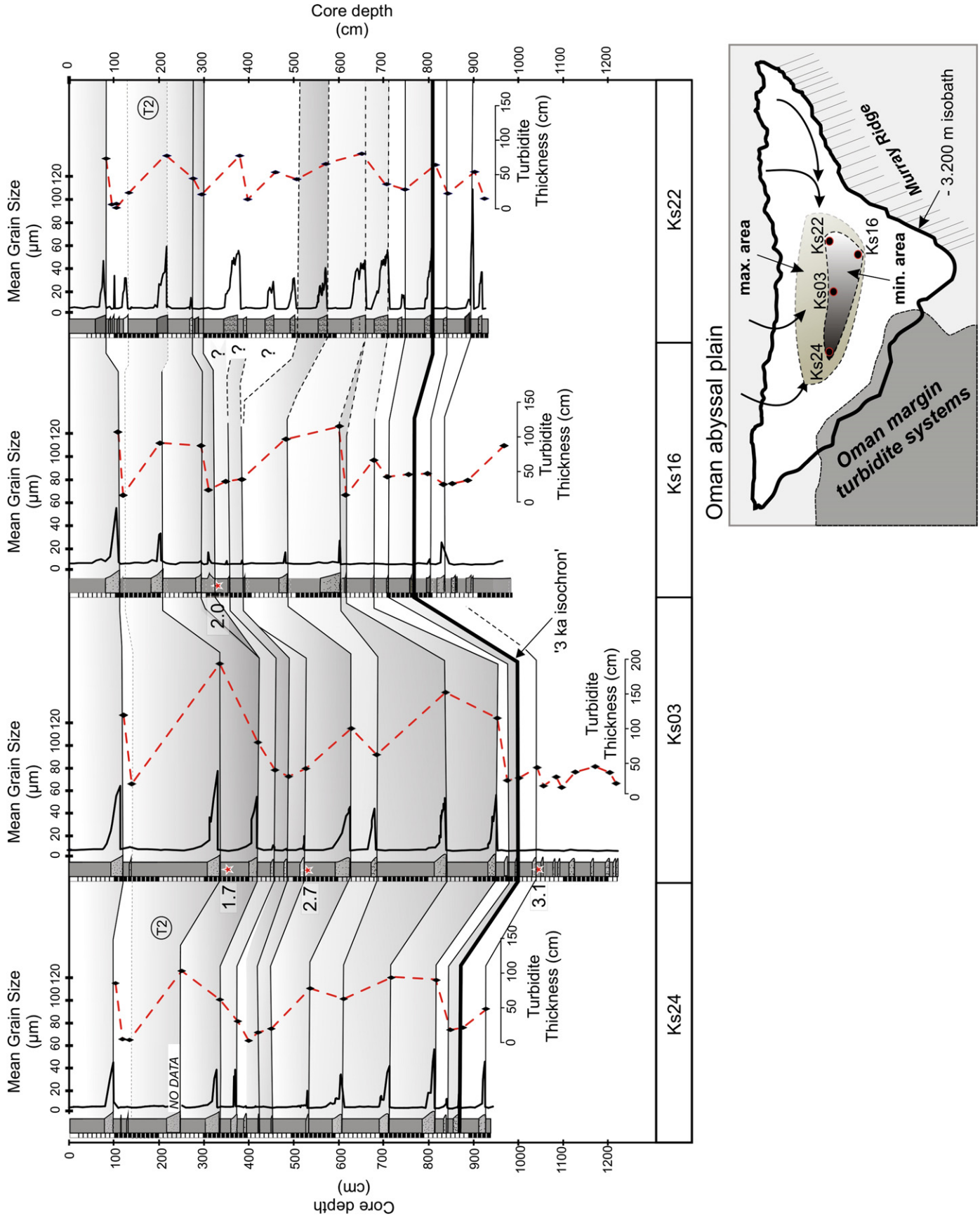
Core depth (cm)
Mean Grain Size (μm)
Turbidite Thickness (cm)
T2
NO DATA
1.7
2.0
2.7
3.1
'3 ka isochron'
Ks24
Ks03
Ks16
Ks22
Oman abyssal plain
max. area
min. area
Murray Ridge
- 3.200 m isobath
Oman margin turbidite systems

floods, as suggested by the observation of rare hyperpycnite beds in the abyssal plain (Bourget et al., in press).

The Makran area is also an area of important tsunami generation related to seismic activity, and is the second zone in importance in the Indian Ocean after Indonesia (Heidarzadeh et al., 2009). The tsunami associated with the 1945 Makran earthquake event (Fig. 1) caused 4000 casualties and have been reported along the Oman, northern Indian, and even Seychelles coasts (Ambraseys and Melville, 1982; Byrne et al., 1992). Numerical modelling of tsunami wave generation and propagation showed that vertical movements associated with co-seismic uplift were not sufficient to explain the wave heights reported by local, direct measurements (Heidarzadeh, pers. comm.). In addition, several tsunamis waves were reported in Karachi after the mainshock, and the largest damaging waves arrived in Pasni about 1.5, 2.0 and 3.25 h later (Bilham et al., 2007). The most likely explanation for these repetitions and delay is that tsunami waves were triggered, at least partly, by several and successive earthquake-triggered submarine landslides (Ambraseys and Melville, 1982; Byrne et al., 1992; Bilham et al., 2007). This is congruent with our hypothesis of formation of the large volume, multi-sourced co-seismic turbidity currents during the late Holocene. If we assume that earthquake-triggered submarine landslides are an important mechanism for tsunami generation in the area, this also suggests that the late Holocene turbidite record of (at least) the deep Oman abyssal plain (where the co-seismic turbidity currents converge) should be representative of the tsunami history in the Arabian Sea. As the historical continental record is sparse, this late Holocene marine archive, better constrained by additional coring sites and stratigraphic resolution, might be valuable to evaluate the seismic and tsunami hazard for the populated Makran coast and the cities of Karachi and Muscat.

5.3. Control parameters on turbidite sedimentation in Late Quaternary monsoon-influenced margins: comparison with the Nile and Indus turbidite systems

Evaluating the growth of the Makran turbidite system during the last glacio-eustatic cycle allow us to focus on the relative importance and the interactions between the main external controls on deep-sea sedimentation, on a high-resolution time scale (<20 ka). Classical models of sequence stratigraphy and more recent 3D seismic-reflection observations of stratigraphic successions in marine environments suggest a systematic development of deep-water sequences mainly related to relative sea-level fluctuations (Vail and Mitchum, 1977; Posamentier et al., 1989; Kolla, 1993; Posamentier and Kolla, 2003). This leads to the conception of an idealized high-resolution stratigraphic model, thought to be cyclic and widely applicable for deep-water exploration (Posamentier and Kolla, 2003). However, previously cited models have been built without absolute dating of the sedimentary successions which may have led to uncertainties and assumptions about the timing of sedimentation. Furthermore, relative sea-level control can vary depending on the local basin setting and physiographic context. Typically, small to mid-size turbidite systems associated with narrow shelves can be strongly influenced by local hydro-climatic parameters (such as hyperpycnal flows, interceptions by canyons of active longshore drift, or a combination of them). This lead to active turbidite system activity during highstands conditions, well illustrated in the California borderland fans (Piper et al., 1999; Covault et al., 2007; Romans et al., 2009) or the Var turbidite system (Mulder et al., 1998). Minor but effective highstand turbidite activity is also observed in large, mud-rich turbidite systems where canyons deeply incise the shelf and are still located close to the river mouth (i.e. the Zaire or Bengal fans; Babonneau et al., 2002; Curray et al., 2002). We showed that in the case of the Makran active margin, timing of turbidite system growth differs from other deep-water systems because the sea-level control is modulated by the high-resolution climate-induced changes in sediment supply stacked with the tectonic influence (continental uplift, earthquakes). Here we propose to assess the role of these interacting forcings on Makran turbidite sedimentation, and to compare it with the Nile and Indus turbidite systems (Fig. 11). These two large delta-fed turbidite systems are located in very different basin contexts, but they have been theoretically influenced by the same monsoon climate and sea-level changes during the late Quaternary (Fig. 11). They thus provide an interesting opportunity to use modern analogues to investigate the impact of shared forcing parameters on the growth of turbidite systems.

5.3.1. Basin configuration

The first parameters to consider when investigating the mechanisms and timing of sediment transfer to deep water are the characteristics of continental drainage basin and the receiving basin setting. The Makran turbidite system displays a typical setting of an active margin, fed by numerous intermittent coastal streams (50–100 km long, <500 km^2 drainage basins) and more perennial mountainous rivers to the east (about 300 km long and $10 \cdot 10^3$–$40 \cdot 10^3$ km^2 drainage basins). Sediment is supplied to the sea through sporadic flash-floods of the Makran Rivers, carrying very large amounts of bulk material to the narrow (20–40 km) shelf (von Rad et al., 1999a; Luckge et al., 2001). The adjacent Indus River develops on 3180 km long, with a $1.2 \cdot 10^6$ km^2 drainage basin composed by the Himalayan mountains and glaciers (Clift et al., 2002). It is characterized by 1350 km long, flat floodplain. The continental shelf is about 100 km wide off the river mouth. The Nile River forms an even much bigger system and develops on 6825 km long, with a $2.8 \cdot 10^6$ km^2 drainage basin, flowing along a flat, 3000 km long arid floodplain. The continental shelf size is variable, but is less than 40 km wide upstream of the last active canyon and channel/levee systems (CLS; Ducassou et al., 2009). Each of those systems showed different response for similar climate and glacio-eustatic changes during the late Quaternary (Fig. 11).

5.3.2. Relative importance of forcing parameters

Sea-level changes primarily control the shifting of depocenters towards the shelf-edge and the possibilities of direct transfer of sediments from rivers to deep-water (Posamentier et al., 1991; Posamentier and Kolla, 2003). However, the example of the Makran and Nile margins show that climate can significantly punctuate the timing and nature of turbidite systems growth at millennial time scales. In that case, the resulting stratigraphic architecture cannot be directly linked to sea-level changes. Monsoon-induced periods of continental aridity and humidity have major impact on fluvial environment dynamics (Blum and Törnqvist, 2000; Jain and Tandon, 2003). For a given substrate, climate appears as a first-order control on the sand-to-mud ratio in the watershed and at river mouths (Perlmutter and Mattews, 1989; Blum and Törnqvist, 2000). Continental aridity during the weak monsoon, LGM period, led to increased production of coarse-grained sediments (due to the lack of vegetation) in both the Nile (Ducassou et al., 2009) and the Makran rivers settings (Fig. 11). Both turbidite systems were dominated by sand-rich, thinner turbidity currents during this period (Fig. 11). Classically, falling and lowstand of sea-level in the Nile turbidite system during

Fig. 10. Sedimentary logs, mean grain size data (μm) and turbidite thickness (cm) of the sedimentary cores from the Oman abyssal plain (modified from Bourget et al., in press). Red stars indicate the radiocarbon ages (Table 2). Turbidite beds mainly consist of thick, sheet-like mud-rich turbidites of late Holocene age (last ~3 ka), correlated on a 4189 km^2 (minimum) area. The total surface area of the Oman abyssal plain (where the sheet-like turbidites may occur, estimated from the present-day isobaths) is about 15 000 km^2 (maximum area).

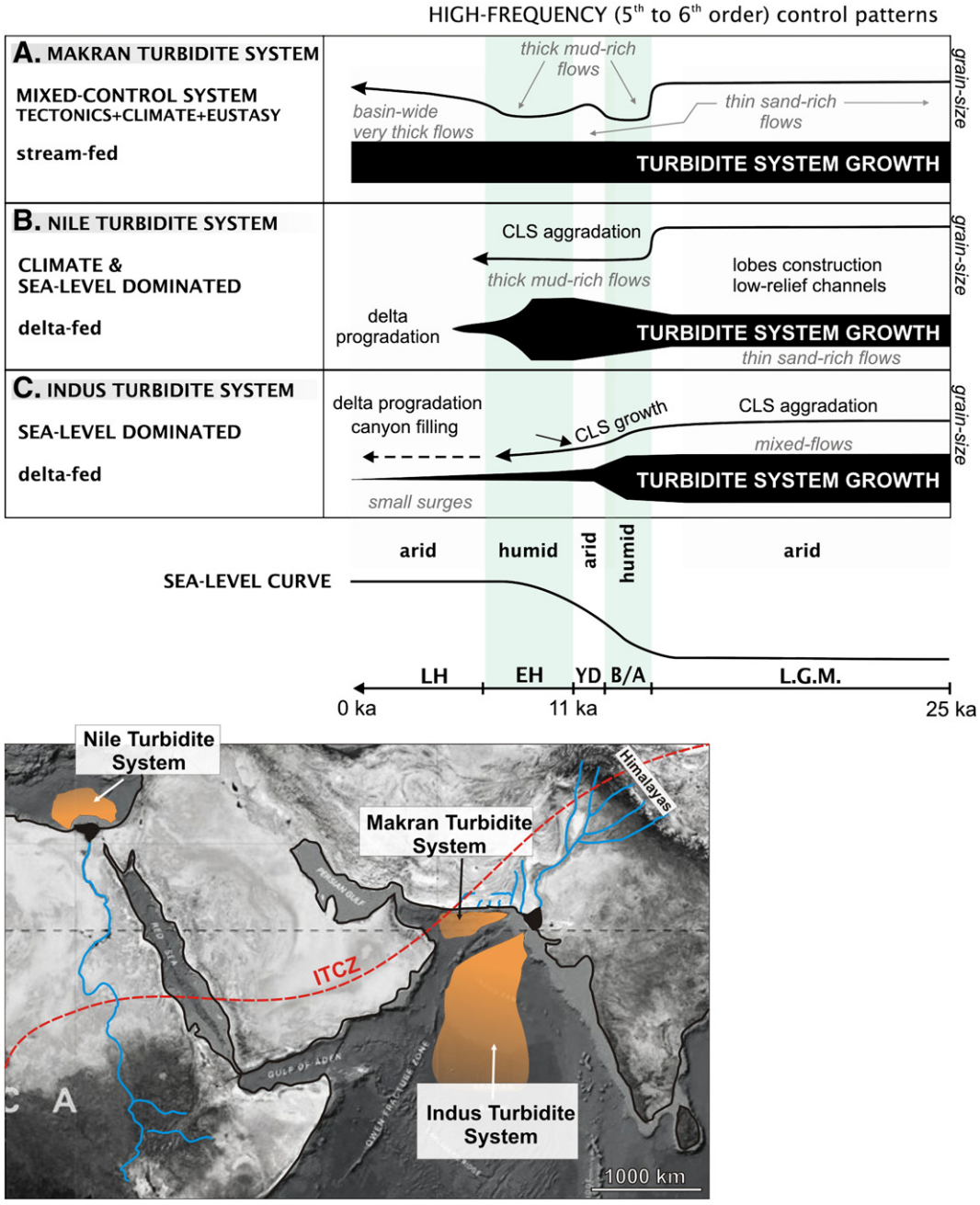

Fig. 11. Simplified model for late Quaternary turbidite system growth and external controls patterns at high-frequency (5th to 6th orders) stratigraphic time scales, in the Makran (A; this study), Nile (B; Ducassou et al., 2009) and Indus (C; von Rad and Tahir, 1997; Prins et al., 2000a) turbidite systems. Sea-level curve simplified from Siddall et al. (2003). Location of each turbidite systems and relative position of the summer ITCZ (InterTropical Convergence Zone) from Fleitmann et al. (2007). Relative sea-level curve is simplified from Fairbanks (1989) and Siddall et al. (2003).

the LGM has been associated with shelf incision and turbidite system initiation. However, it was characterized by sand-rich, low relief levees, with overall low sedimentation rates (Ducassou et al., 2009). This is attributed to a net decrease in fluvial discharge (Blum and Törnqvist, 2000) associated with aggradation and storage of sediments in the drainage basin, along the 3000 km long, flat floodplain of the Nile River (Ducassou et al., 2009). Similar decrease in water flux and transport capacity of the Makran rivers during the LGM was probably compensated by the occasional flooding of the shorter, higher-gradients river systems, which allowed an active transfer of bulk material directly to the shelf-edge and canyons, and subsequent very active turbidite system growth (Fig. 11). Hence, the Makran and Nile turbidite systems were both dominated by sand-rich material during the LGM arid period, but the size of the rivers and type of watersheds led to differences in rates of deep-water sediment accumulation. In the Indus turbidite system, channel/levee system (CLS) avulsion and increasing sediment transfer to the basin occurred during the last sea-level fall (at about ~30 ka BP), contemporaneously to canyon erosion through Indus River incision on the shelf (von Rad and Tahir, 1997; Prins and Postma, 2000; Prins et al., 2000a). During the LGM lowstand, the Indus River was directly connected to a mature, well developed canyon, leading to very active CLS construction and levee aggradation related to frequent, sand and mud rich (mixed), thick turbidity currents (von Rad and Tahir, 1997; Prins et al., 2000a). Hence, the Indus turbidite system has been less influenced by the continental aridity during the LGM (Fig. 11).

The early stages of sea-level rise (after ~19 ka BP) were associated with persistent CLS growth in the Indus fan (Prins et al., 2000a),

possibly through increasing water and sediment flux due to post-glacial melting of Himalayan ice-sheets (Prins et al., 2000a) as well as increasing monsoon-related precipitations at the beginning of the Bölling–Alleröd (Schulz et al., 1998). However, immersion of the continental shelf above a certain threshold (about −70 m) after 13–14 ka BP led to retreat of fluvial input, trapping of sediments on the continental shelf, and starvation of the CLS (von Rad and Tahir, 1997; Prins et al., 2000a; Fig. 11). Contemporaneously, increased water and fine-grained sediment discharge from rivers in a more humid climate (Gasse, 2000; Jain and Tandon, 2003; Fleitmann et al., 2007) led to very active Makran and Nile turbidite systems growth (Fig. 11). Sedimentation in these systems was dominated by frequent, thick mud-rich turbidity currents (Fig. 11). In the Nile turbidite system, fine-grained turbidites and flood-related muds caused aggradation of high-relief, muddy leveed-channels with high sedimentation rates (Ducassou et al., 2009). Our data suggests that the short-term return to arid conditions during the Younger Dryas was associated with an instantaneous response in the Makran turbidite system (i.e. a less than 3000 yr return to thinner, coarser-grained flows). The latter is not recorded in the Nile turbidite system (Fig. 11), either because small streams are more sensitive to climate change and have very small response times and geomorphic thresholds as compared to larger fluvial systems (Paola et al., 1992; Jain and Tandon, 2003), or because of the lower stratigraphic resolution in the Nile sediments (Ducassou et al., 2009). However, the relatively narrow shelves of both the Makran and Nile turbidite systems allowed the climate-induced increase in sediment supply to compensate the effect of rising sea-level, while the large shelf at the Indus River mouth promoted trapping of sediments in staging area (von Rad and Tahir, 1997; Fig. 11).

Finally, the onset of maximum sea-level after ~7 ka BP was associated with trapping of the Nile River sediments on the shelf and in the delta, and starvation of the turbidite system (Fig. 11). Minor highstand turbidite activity may occur in the proximal Indus turbidite system (canyon-fill; Fig. 11) due to the incision of the Indus canyon at −20 m water depth close to the present-day shoreline (von Rad and Tahir, 1997; Prins et al., 2000a). However, more than 85% of the 250 million tons of sediment estimated to be discharged annually by the Indus River are trapped in the inner to mid-shelf highly prograding clinoforms (Giosan et al., 2006). Sea-level highstand also promotes sediment accumulation on the narrow Makran shelf and upper slope, associated with very high sedimentation rates (Fig. 9). However, the rare (~200 yr) failure-induced purge events enhance transfer of huge volumes of sediments in the deep basin (Fig. 11). Cores from the deep Oman abyssal plain show a mean value of 8.59 m of turbidite sediments deposited during the last ~3 ka (Fig. 10). Based on the surface area of 4189 km^2 calculated from the cores position, the minimum bulk sediment volume accumulated in the abyssal plain in 3000 yr is 35.9 km^3 (11.9 $km^3 ka^{-1}$). Considering the probable area of deposition of the thick, sheet-like turbidites in the abyssal plain (~15,000 km^2; Fig. 10), the maximum bulk sediment volume estimation reach 129 km^3 (42.9 $km^3 ka^{-1}$). As we do not consider here the canyon mouths and proximal trench areas, this total volume of sediment accumulated during this 3 ka highstand period is a minimum and likely significantly underestimated.

For similar climate and sea-level histories, differences in the timing and rates of sediment supply in these three deep-water systems can be considered in terms of drainage basin morphology (fluvial dynamics), its sensitivity to high-frequency (climate-driven) sediment flux variability, continental shelf extension (basin morphology), and tectonic setting. The Indus turbidite system evolution is analogous to the idealized, sea-level controlled-model for turbidite system growth (Posamentier and Kolla, 2003), which consider no major change in sediment flux at river outlets at high-frequency and shelf-dominated highstand sedimentation (Fig. 11). In this context, the Nile turbidite system can be considered as an intermediate delta-fed system (Fig. 11) where both eustasy and climate interact, leading to significantly different stratigraphic successions in comparison to others large, delta-fed turbidite systems such as the Amazon fan (Flood et al., 1991). Conversely, the Makran convergent margin forms a typical example of mixed-controlled sedimentary system where tectonics, climate and eustasy interplay at high-frequency (<20 ka) cycles (Fig. 11). The large volumes of highstand turbidite deposits accumulated in the basin are clearly as significant as lowstand deposits in the geologic record. This can complicate the interpretation of high-resolution sedimentary successions in buried or outcrop systems with similar geodynamic context and paleo-physiography—typically, turbidite-filled thrust-belts, wedge top and foredeep depozones in ancient foreland basins (Mutti et al., 2003).

6. Conclusions

Late Quaternary Makran turbidite system growth has been continuous throughout the sea-level lowstand, transgressive, and highstand conditions. However, the frequency, rates, and nature of sediment supply varied through the last ~25 ka BP, in response to climate, sea level, and tectonically induced changes in "source-to-sink" sediment dispersal modes. These changes include conditions of sediment production and availability in the drainage basin, capacity of transport from fluvial systems, and rates of sediment storage on the shelf and upperslope areas.

Climate in the hinterland appears as a first-order control on the fluvial dynamics and on the resulting properties of turbidity currents that feed the turbidite system, controlling the average sand-to-mud ratio in the resulting deposits. Arid conditions were associated with sand-rich turbidity currents resulting in thin, fine sand-basal turbidite deposition in the abyssal plain. Inversely, wetter periods were associated with frequent thicker (>300 m), mud-rich turbidity currents and thin, fine-grained (silt-mud) turbidites, relative to enhanced fluvial discharge and development of vegetation cover in the catchment. A steep slope and a shelf break at ~20–50 m water depth prevented shelf immersion after the LGM lowstand, during the rising sea-level and the early Holocene, allowing high rates of turbidite system growth in both arid and humid conditions. Onset of sea-level highstand after ~8 ka BP mark an obvious change in turbidite system growth, characterized by the occurrence of thicker turbidite beds elsewhere in the Makran continental slope and abyssal plain. These deposits show an important decrease in recurrence time interval, which range from ~100 yr (in the canyon axis) to ~200 years (in most of depositional environments); i.e. close to the time recurrence for the large magnitude earthquakes in the Makran coastal area. Highstand turbidite system growth is generated by the occasional flushing of upper-slope, high accumulation rates muddy sediments into the turbidite system in form of co-seismic, mass-wasting events. In the Holocene turbidite succession, the overall thickness of individual turbidite beds everywhere and the thick mud-rich, sheet-like turbidites deposited in the deep Oman abyssal plain suggest the occurrence of large volume thick turbidity currents originated from successive, multiple slide or slump-induced surges. As earthquake-triggered submarine landslides are an important mechanism for tsunami generation in the area, the Holocene turbidite record of the deep Oman abyssal plain might be representative of the earthquake/tsunami history in the Arabian Sea.

Comparison with the Nile and Indus turbidite system growth during the Late Quaternary permits evaluation of the interplay and the relative importance of shared forcing parameters (i.e. monsoon climate, sea-level cycle) in very different basin settings. While the shelf-dominated Indus fan appears mainly controlled by eustasy during the last 25 ka, similarities are found between the Nile and Makran turbidite systems, where sea-level changes are strongly modulated by the climate impact on fluvial dynamics in the hinterland (sediment production versus discharge ratio). However,

the Makran margin setting promoted a continuous turbidite system growth through time, because both the uplift of the coastal area and the fluvial dynamics of short, mountainous river systems allow high sediment transfer rates to the continental shelf and steep upper slope, even though arid conditions with low water fluxes. Highstand turbidite deposits form a thick sedimentary succession in the Oman abyssal plain with high accumulation rates, and are significant in the geologic record.

Our results show that both the rates and nature of sedimentation along active margins are very sensitive to high-frequency (3–10 ka), climate-induced changes in fluvial discharge and sediment supply, as suggested by analogue modelling (Paola et al., 1992; Van Den Berg Van Saparoea and Postma, 2008). It illustrates how short drainage systems can be very efficient in responding to high-frequency changes in sediment flux and how tectonic forcing acts on turbidite system growth at time scales less than 20 ka. The complex interplay between high-frequency variability and rate of sediment supply at river outlets, relative sea-level change, and local tectonics, influence the frequency, the magnitude, and the sediment composition of the gravity flows and resulting deposits in the basin, producing significant changes in the stratigraphic record at 5th or 6th orders. The Makran turbidite system growth during the late Quaternary is a valuable analogue for the interpretation of high-resolution sedimentary successions in buried or outcrop systems with similar geodynamic context or paleo-physiography, such as ancient foreland basins.

Acknowledgements

We would like to thank IFP and SHOM for making its data available. We are indebted to all scientists, technicians and crew members of the *R/V Le Suroît*, *R/V Atalante* and *R/V Marion-Dufresne* for their technical assistance during the MARABIE and CHAMAK cruises. The authors are also grateful to E. Moreno at the MNHN, and J. St Paul, G. Chabaud and B. Martin (University of Bordeaux) for their logistical and technical assistance. Reviews by Brian Romans, Tor O. Sømme, and co-editor David J. Piper significantly improved the clarity of this paper. We finally acknowledge the 'ARTEMIS' project for radiocarbon dating and the "Action Marges" French Consortium. J.B PhD thesis has been funded by a DGA–CNRS doctoral fellowship. This is an UMR CNRS 5805 EPOC (University Bordeaux 1) contribution n. 1755.

References

Allen, G.P., 2008. Time scales of tectonic landscapes and their sediment routing systems. In: Gallagher, K., Jones, S.J., Wainwright, J. (Eds.), Landscape, Evolution: Denudation, Climate and Tectonics Over Different Time and Space Scales: Geological Society of London Special Publication, pp. 7–28.

Ambraseys, N., Bilham, R., 2003. Earthquakes and associated deformation in Northern Baluchistan 1892–2001. Bulletin of the Seismological Society of America 93 (4), 1573–1605.

Ambraseys, N.N., Melville, C.P., 1982. A History of Persian Earthquakes. Cambridge University Press, Britain.

Babonneau, N., Savoye, B., Cremer, M., Klein, B., 2002. Morphology and architecture of the present canyon and channel system of the Zaire deep-sea fan. Marine and Petroleum Geology 19 (4), 445–467.

Bard, E., 1998. Geochemical and geophysical implications of the radiocarbon calibration. Geochimica Cosmochimica Acta 62, 2025–2038.

Bilham, R., Lodi, S., Hough, S., Bukhary, S., Khan, A.M., Rafeeqi, S.F.A., 2007. Seismic hazard in Karachi, Pakistan: uncertain past, uncertain future. Seismological Research Letters 78 (6), 601–613.

Blum, M.D., Törnqvist, T.E., 2000. Fluvial responses to climate and sea-level change: a review and look forward. Sedimentology 47 (s1), 2–48.

Blumberg, S., Lamy, F., Arz, H.W., Echtler, H.P., Wiedicke, M., Haug, G.H., Onlen, O., 2008. Turbiditic trench deposits at the South-Chilean active margin: a Pleistocene–Holocene record of climate and tectonics. Earth and Planetary Science Letters 268 (3–4), 526–539.

Böning, P., Bard, E., 2009. Millennial/centennial-scale thermocline ventilation changes in the Indian Ocean as reflected by aragonite preservation and geochemical variations in Arabian Sea sediments. Geochimica et Cosmochimica Acta 73, 6771–6788.

Bouma, A.H., 1962. Sedimentology of some flysch deposits: a graphic approach to facies interpretation. Amsterdam, Elsevier. 168 pp.

Bouma, A.H., Coleman, J.H., Stelting, C.E., Kohl, B., 1989. Influence of relative sea level changes on the construction of the Mississippi fan. Geo-Marine Letters 161–170.

Bourget, J., Zaragosi, S., Ellouz-Zimmermann, N., Mouchot, N., Garlan, T., Schneider, J.-L., Lanfumey, V., Lallemant, S., in press. Turbidite system architecture and sedimentary processes along topographically complex slopes: the Makran convergent margin. Sedimentology. doi:10.1111/j.1365-3091.2010.01168.x.

Brami, T.R., Pirmez, C., Archie, C., Holman, K., 2000. Late Pleistocene deep-water stratigraphy and depositional processes, offshore Trinidad and Tobago. In: Weimer, P., et al. (Ed.), Deep-water reservoirs of the world: Gulf Coast Section SEPM 20th Annual Conference, pp. 104–115.

Burns, S.J., Fleitmann, D., Matter, A., Kramers, J., Al-Subbary, A.A., 2003. Indian Ocean climate and an absolute chronology over Dansgaard/Oeschger events 9 to 13. Science 301 (5638), 1365–1367.

Byrne, D.E., Sykes, L.R., Davis, D.M., 1992. Great thrust earthquakes and aseismic slip along the plate boundary of the Makran subduction zone. Journal of Geophysical Research 97, 449–478.

Castelltort, S., Van Den Driessche, J., 2003. How plausible are high-frequency sediment supply-driven cycles in the stratigraphic record? Sedimentary Geology 157 (1–2), 3–13.

Catuneanu, O., Abreu, V., Bhattacharya, J.P., Blum, M.D., Dalrymple, R.W., Eriksson, P.G., Fielding, C.R., Fisher, W.L., Galloway, W.E., Gibling, M.R., Giles, K.A., Holbrook, J.M., Jordan, R., Kendall, C.G., St, C., Macurda, B., Martinsen, O.J., Miall, A.D., Neal, J.E., Nummedal, D., Pomar, L., Posamentier, H.W., Pratt, B.R., Sarg, J.F., Shanley, K.W., Steel, R.J., Strasser, A., Tucker, M.E., Winker, C., 2009. Towards the standardization of sequence stratigraphy. Earth-Science Reviews 92 (1–2), 1–33.

Clemens, S.C., Prell, W.L., 2003. A 350,000 year summer-monsoon multi-proxy stack from the Owen Ridge, Northern Arabian Sea. Marine Geology 201 (1–3), 35–51.

Clemens, S.C., Prell, W.L., 2007. The timing of orbital-scale Indian monsoon changes. Quaternary Science Reviews 26 (3–4), 275–278.

Clemens, S., Wang, P., Prell, W., 2003. Monsoons and global linkages on Milankovitch and sub-Milankovitch time scales. Marine Geology 201 (1–3), 1–3.

Clift, P., Gaedicke, C., Edwards, R., Lee, J.I., Hildebrand, P., Amjad, S., White, R.S., Schlüter, H.-U., 2002. The stratigraphic evolution of the Indus fan and the history of sedimentation in the Arabian Sea. Marine Geophysical Researches 23, 223–245.

Covault, J.A., Normark, W.R., Romans, B.W., Graham, S.A., 2007. Highstand fans in the California borderland: the overlooked deep-water depositional systems. Geology 35 (9), 783–786.

Curray, J.R., Emmel, F.J., Moore, D.G., 2002. The Bengal Fan: morphology, geometry, stratigraphy, history and processes. Marine and Petroleum Geology 19 (10), 1191–1223.

DeMets, C., Gordon, R.G., Angus, D.F., Stein, S., 1994. Effect of recent revisions to the geomagnetic reversal time scale on estimates of current plate motions. Geophysical Research Letters 21 (20), 2191–2194.

Ducassou, E., Migeon, S., Mulder, T., Murat, A., Capotondi, L., Bernasconi, S.M., Mascle, J., 2009. Evolution of the Nile Deep-Sea turbidite system during the Late Quaternary: influence of climate change on fan sedimentation. Sedimentology 56, 2061–2090.

Ellouz-Zimmermann, N., Deville, E., Muller, C., Lallemant, S.J., Subhani, A.B., Tabreez, A.R., 2007a. Impact of sedimentation on convergent margin tectonics: example of the Makran accretionary prism. In: Lacombe, O., Lavé, J., Roure, F., Verges, J. (Eds.), Thrust Belts and Foreland Basins.

Ellouz-Zimmermann, N., Lallemant, S., Castilla, R., Mouchot, N., Leturmy, P., Battani, A., Buret, C., Cherel, L., Desaubliaux, G., Deville, E., Ferrand, J., Lügcke, A., Mahieux, G., Mascle, G., Mühr, P., Pierson-Wickmann, A., Robion, P., Schmitz, J., Danish, M., Hasany, S., Shahzad, A., Tabreez, A., 2007b. Offshore frontal part of the Makran Accretionary prism: the Chamak Survey (Pakistan), thrust belts and foreland basins, pp. 351–366.

Ercilla, G., Alonso, B., Wynn, R.B., Baraza, J., 2002. Turbidity current sediment waves on irregular slopes: observations from the Orinoco sediment-wave field. Marine Geology 192 (1–3), 171–187.

Fairbanks, G., 1989. A 17, 000-year blacio-eustatic sea level record/influence of glacial melting rates on the Younger Dryas event and deep-ocean circulation. Nature 342, 637–642.

Fleitmann, D., Burns, S.J., Mangini, A., Mudelsee, M., Kramers, J., Villa, I., Neff, U., Al-Subbary, A.A., Buettner, A., Hippler, D., Matter, D., 2007. Holocene ITCZ and Indian monsoon dynamics recorded in stalagmites from Oman and Yemen (Socotra). Quaternary Science Reviews 26 (1–2), 170–188.

Flood, R.C., Manley, P.L., Kowsmann, K.O., Appi, C.J., Pirmez, C., 1991. Seismic facies and late Quaternary growth of Amazon submarine fan. In: Weimer, P., Link, M.H. (Eds.), Seismic Facies and Sedimentary Processes of Submarine Fans and Turbidite Systems. Springer-Verlag, NewYork, pp. 415–434.

Flueh, E.R., Kukowski, N., Reichert, C., 1997. RV Sonne, Cruise Report SO123 'MAMUT' (Makran Murray Traverse): GEOMAR Report, vol. 62. 291pp.

Fruehn, J., White, R.S., Minshull, T.A., 1997. Internal deformation and compaction of the Makran accretionary wedge. Terra Nova 9 (3), 101–104.

Garziglia, S., Migeon, S., Ducassou, E., Loncke, L., Mascle, J., 2008. Mass-transport deposits on the Rosetta province (NW Nile deep-sea turbidite system, Egyptian margin): characteristics, distribution, and potential causal processes. Marine Geology 250 (1–4), 180–198.

Gasse, F., 2000. Hydrological changes in the African tropics since the Last Glacial Maximum. Quaternary Science Reviews 19 (1–5), 189–211.

Giosan, L., Constantinescu, S., Clift, P.D., Tabrez, A.R., Danish, M., Inam, A., 2006. Recent morphodynamics of the Indus delta shore and shelf. Continental Shelf Research 26 (14), 1668–1684.

Glennie, K.W., Singhvi, A.K., 2002. Event stratigraphy, paleoenvironment and chronology of SE Arabian deserts. Quaternary Science Reviews 21 (7), 853–869.

Goldfinger, C., Nelson, C.H., Johnson, J.E., Scientific Party, T.S., 2003. Holocene earthquake records from the Cascadia subduction zone and northern San Andreas fault based on precise dating of offshore turbidites. Annual Review of Earth and Planteray Sciences 31, 55–77.
Goldfinger, C., Morey, A.E., Nelson, C.H., Gutiérrez-Pastor, J., Johnson, J.E., Karabanov, E., Chaytor, J., Eriksson, A., 2007. Rupture lengths and temporal history of significant earthquakes on the offshore and north coast segments of the Northern San Andreas Fault based on turbidite stratigraphy. Earth and Planetary Science Letters 254 (1–2), 9–27.
Grando, G., McClay, K., 2007. Morphotectonics domains and structural styles in the Makran accretionary prism, offshore Iran. Sedimentary Geology 196 (1–4), 157–179.
Gupta, A.K., Anderson, D.M., Overpeck, J.T., 2003. Abrupt changes in the Asian southwest monsoon during the Holocene and their links to the North Atlantic Ocean. Nature 421, 354–357.
Heidarzadeh, M., Pirooz, M., Zaker, N., Yalciner, A., 2009. Preliminary estimation of the tsunami hazards associated with the Makran subduction zone at the northwestern Indian Ocean. Natural Hazards 48 (2).
Hosseini-Barzi, M., Talbot, C., 2003. A tectonic pulse in the Makran accretionary prism recorded in Iranian coastal sediments. Journal of the Geological Society, London 160, 903–910.
Ivanochko, T.S., Ganeshram, R.S., Brummer, G.A., Ganssen, G., Jung, S.J.A., Moreton, S.G., Kroon, D., 2005. Variations in tropical convection as an amplifier of global climate change at the millennial scale. Earth and Planetary Science Letters 235 (1–2), 302–314.
Ivory, S.J., Lézine, A.-M., 2009. Climate and environmental change at the end of the Holocene Humid Period: a pollen record off Pakistan. Comptes Rendus Geosciences 341 (8–9), 760–769.
Jain, M., Tandon, S.K., 2003. Fluvial response to Late Quaternary climate changes, western India. Quaternary Science Reviews 22 (20), 2223–2235.
Juyal, N., Chamyal, L.S., Bhandari, S., Bhushan, R., Singhvi, A.K., 2006. Continental record of the southwest monsoon during the last 130 ka: evidence from the southern margin of the Thar Desert, India. Quaternary Science Reviews 25 (19–20), 2632–2650.
Klöcker, R., Henrich, R., 2006. Recent and Late Quaternary pteropod preservation on the Pakistan shelf and continental slope. Marine Geology 231 (1–4), 103–111.
Kneller, B.C., 1995. Beyond the turbidite paradigm: physical models for deposition of turbidites and their implications for reservoir prediction. In: Hartley, A.J., Prosser, D.J. (Eds.), Characterization of Deep Marine Clastic Systems: Geological Society Special Publication, pp. 31–49.
Kolla, V., 1993. Lowstand deep-water siliciclastic depositional system: characteristics and terminologies in sequence stratigraphy and sedimentology. Bulletin des Centres de Recherches Exploration–Production Elf-Aquitaine 67–78.
Kukowski, N., Schillhorn, T., Huhn, K., von Rad, U., Husen, S., Flueh, E., 2001. Morphotectonics and mechanics of the central Makran accretionary wedge off Pakistan. Marine Geology 173 (1–4), 1–19.
Laronne, J.B., Reid, L., 1993. Very high rates of bedload sediment transport by ephemeral desert rivers. Nature 366 (6451), 148–150.
Leuschner, D.C., Sirocko, F., 2003. Orbital insolation forcing of the Indian Monsoon—a motor for global climate changes? Palaeogeography, Palaeoclimatology, Palaeoecology 197 (1–2), 83–95.
Lowe, D.R., 1982. Sediment gravity flows: II. Depositional models with special reference to the deposits of high-density turbidity currents. Journal of Sedimentary Petrology 52 (1), 279–297.
Luckge, A., Doose-Rolinski, H., Khan, A.A., Schulz, H., von Rad, U., 2001. Monsoonal variability in the northeastern Arabian Sea during the past 5000-years: geochemical evidence from laminated sediments. Palaeogeography, Palaeoclimatology, Palaeoecology 167 (3–4), 273–286.
Migeon, S., Weber, O., Faugères, J.C., Saint-Paul, J., 1999. SCOPIX: a new imaging system for core analysis. Geo-Marine Letters 18, 251–255.
Migeon, S., Savoye, B., Zanella, E., Mulder, T., Faugeres, J.-C., Weber, O., 2001. Detailed seismic-reflection and sedimentary study of turbidite sediment waves on the Var Sedimentary Ridge (SE France): significance for sediment transport and deposition and for the mechanisms of sediment-wave construction. Marine and Petroleum Geology 18, 179–208.
Milliman, J.D., Syvitski, J.P.M., 1992. Geomorphic/tectonic control of sediment discharge to the ocean: the importance of small mountainous rivers. Journal of Geology 100, 525–544.
Mouchot, N., Loncke, L., Mahieux, G., Bourget, J., Lallemant, S., Ellouz-Zimmermann, N., Leturmy, P., 2010. Recent sedimentary processes along the Makran trench (Makran active margin, off Pakistan). Marine Geology 271 (1–2), 17–31.
Mulder, T., Alexander, J., 2001. The physical character of subaqueous sedimentary density flow and their deposits. Sedimentology 48 (2), 269–299.
Mulder, T., Savoye, B., Piper, D.J.W., Syvitski, J.P.M., 1998. The Var submarine sedimentary system: understanding Holocene sediment delivery processes and their importance to the geological record. In: Stocker, M.S., Evans, D., Cramp, A. (Eds.), Geological processes on continental margins: sedimentation, mass-wasting and stability: Geological Society, London, Special Publications, pp. 146–166.
Mutti, E., Lucchi, F.R., Seguret, M., Zanzucchi, G., 1984. Seismoturbidites: a new group of resedimented deposits. Marine Geology 55 (1–2), 103–116.
Mutti, E., Tinterri, R., Benevelli, G., Biase, D., Cavanna, G., 2003. Deltaic, mixed and turbidite sedimentation of ancient foreland basins. Marine and Petroleum Geology 20 (6–8), 733–755.
Nakajima, T., Kanai, Y., 2000. Sedimentary features of seismoturbidites triggered by the 1983 and older historical earthquakes in the eastern margin of the Japan Sea. Sedimentary Geology 135 (1–4), 1–19.
Page, W.D., Alt, J.N., Cliff, L.S., Plafker, G., 1979. Evidence for occurrence of large magnitude earthquakes along the Makran coast of Iran and Pakistan. Tectonophysics 52, 533–547.
Paola, C., Heller, P.L., Angevinet, C.L., 1992. The large-scale dynamics of grain-size variations in alluvial basins, 1. Theory Basin Research 4, 73–90.
Parker, G., 1982. Conditions for the ignition of catastrophically erosive turbidity currents. Marine Geology 307–327.
Perlmutter, M.A., Mattews, M.D., 1989. Global cyclostratigraphy—a model. In: Cross, T.A. (Ed.), Quantitative Dynamic Stratigraphy. Prentice-Hall, Englewood Cliffs, pp. 233–260.
Piper, D.J.W., Aksu, A.E., 1987. The source and origin of the 1929 Grand Banks turbidity current inferred from sediment budget. Geo-Marine Letters 177–182.
Piper, D.J.W., Normark, W.R., 2009. Processes that initiate turbidity currents and their influence on turbidites: a marine geology perspective. Journal of Sedimentary Research 79 (6), 347–362.
Piper, D.J.W., Shor, A.N., Clarke, J.E.H., 1988. The 1929 "Grand Banks" earthquake, slump, and turbidity current: Geological Society of America Special Paper, pp. 77–92.
Piper, D.J.W., Hiscott, R.N., Normark, W.R., 1999. Outcrop-scale acoustic facies analysis and latest Quaternary development of Hueneme and Dume submarine fans, offshore California. Sedimentology 46 (1), 47–78.
Platt, J.P., Leggett, J.K., Young, J., Raza, H., Alam, S., 1985. Large-scale sediment underplating in the Makran accretionary prism, Southwest Pakistan. Geology 13 (7), 507–511.
Posamentier, H.W., Kolla, V., 2003. Seismic geomorphology and stratigraphy of depositional elements in deep-water settings. Journal of Sedimentary Research 73 (3), 367–388.
Posamentier, H.W., Vail, P.R., 1989. Eustatic controls on clastic deposition II—sequence and systems tract models. Sea-level Changes: An Integrated Approach: In: Wilgus, et al. (Ed.), SEPM Special Publication, Tulsa, pp. 125–154.
Posamentier, H.W., Jervey, M.T., Vail, P.R., 1989. Eustatic controls on clastic deposition I—conceptual framework. Sea-level Changes: An Integrated Approach: In: Wilgus, et al. (Ed.), SEPM Special Publication, Tulsa, pp. 110–124.
Posamentier, H.W., Erskine, R.D., Mitchum, R.M.J., 1991. Models for submarine-fan deposition within a sequence-stratigraphic framework. In: Weimer, P., Link, M.H. (Eds.), Seismic Facies and Sedimentary Processes of Submarine Fans and Turbidite Systems. Spring-Verlag, New York, pp. 127–136.
Posamentier, H.W., Allen, G.P., James, D.P., Tesson, M., 1992. Forced regressions in a sequence stratigraphic framework: concepts, examples, and exploration significance. AAPG Bulletin 76 (11), 1687–1709.
Pourmand, A., Marcantonio, F., Schulz, H., 2004. Variations in productivity and eolian fluxes in the northeastern Arabian Sea during the past 110 ka. Earth and Planetary Science Letters 221 (1–4), 39–54.
Prins, M.A., Postma, G., 2000. Effects of climate, sea level, and tectonics unraveled for last deglaciation turbidite records of the Arabian Sea. Geology 375–378.
Prins, M.A., Postma, G., Cleveringa, J., Cramp, A., Kenyon, N.H., 2000a. Controls on terrigenous sediment supply to the Arabian Sea during the late Quaternary: the Indus Fan. Marine Geology 169 (3–4), 327–349.
Prins, M.A., Postma, G., Weltje, G.J., 2000b. Controls on terrigenous sediment supply to the Arabian Sea during the late Quaternary: the Makran continental slope. Marine Geology 169 (3–4), 351–371.
Quittmeyer, R.C., 1979. Seismicity variations in the Makran region of Pakistan and Iran: relation to great earthquakes. Pure and Applied Geophysics 117 (6), 1212–1228.
Radies, D., Preusser, F., Matter, A., Mange, M., 2004. Eustatic and climatic controls on the development of the Wahiba Sand Sea, Sultanate of Oman. Sedimentology 51 (6), 1359–1385.
Reichart, G.J., Lourens, L.J., Zachariasse, W.J., 1998. Temporal variability in the northern Arabian Sea oxygen minimum zone (OMZ) during the last 225, 000 years. Paleoceanography 13, 607–621.
Reichart, G.J., Schenau, S.J., de Lange, G.J., Zachariasse, W.J., 2002. Synchroneity of oxygen minimum zone intensity on the Oman and Pakistan Margins at sub-Milankovitch time scales. Marine Geology 185 (3–4), 403–415.
Reyss, J.L., Pirazzoli, P.A., Haghipour, A., Hatte, C., Fontugne, M., 1998. Quaternary marine terraces and tectonic uplift rates on the south coast of Iran. In: Stewart, I.S., Vita-Finzi, C. (Eds.), Coastal Tectonics: Geological Society of London, Special Publications, pp. 225–237.
Richards, M., Bowman, M., Reading, H., 1998. Submarine-fan systems I: characterization and stratigraphic prediction. Marine and Petroleum Geology 15 (7), 689–717.
Romans, B.W., Normark, B., McGann, M.M., Covault, J.A., Graham, S.A., 2009. Coarse-grained sediment delivery and distribution in the Holocene Santa Monica Basin, California: implications for evaluating source-to-sink flux at millennial time scales. GSA Bulletin 121, 1394–1408.
Ruddiman, W.F., 2006. What is the timing of orbital-scale monsoon changes? Quaternary Science Reviews 25, 657–658.
Sanlaville, P., Besenval, R., Evin, J., Prieur, A., 1991. Evolution de la région littorale du Makran Pakistanais à l'Holocène Paléorient, 17(1): 3–18.
Schulz, H., Von Rad, U., Erlenkeuser, H., 1998. Correlation between Arabian Sea and Greenland climate oscillayions of the past 110,000 years. Nature 393.
Shiki, T., Cita, M.B., Gorsline, D.S., 2000. Sedimentary features of the seismo-turbidites, Lake Biwa, Japan. Sedimentary Geology 135 (1–4), 37–50.
Siddall, M., Rohling, E.J., Almogi-Labin, A., Hemleben, C., Meischner, D., Schmelzer, I., Smeed, D.A., 2003. Sea-level fluctuations during the last glacial cycle. Nature 423 (6942), 853–858.
Sirocko, F., Sarnthein, M., Lange, H., Erlenkeuser, H., 1991. Atmospheric summer circulation and coastal upwelling in the Arabian Sea during the Holocene and the last glaciation. Quaternary Research 36 (1), 72–93.
Sirocko, F., Garbe-Schonberg, D., McIntyre, A., Molcno, B., 1996. Teleconnections between the subtropical monsoons and high-latitude climates during the last deglaciation. Science 272, 526–529.
Sirocko, F., Garbe-Schonberg, D., Devey, C., 2000. Processes controlling trace element geochemistry of Arabian Sea sediments during the last 25,000 years. Global and Planetary Change 26 (1–3), 217–303.

Skene, K.I., Piper, D.J.W., 2003. Late Quaternary stratigraphy of Laurentian Fan: a record of events off the eastern Canadian continental margin during the last deglacial period. Quaternary International 99–10, 135–152.
Snead, R.E., 1967. Recent morphological changes along the coast of West Pakistan. Annals of the Association of American Geographers 57, 550–565.
Sømme, T.O., Helland-Hansen, W., Martinsen, O.J., Thurmond, J.B., 2009. Relationships between morphological and sedimentological parameters in source-to-sink systems: a basis for predicting semi-quantitative characteristics in subsurface systems. Basin Research 21 (4), 361–387.
Sridhar, A., 2007. Mid-late Holocene hydrological changes in the Mahi River, arid western India. Geomorphology 88 (3–4), 285–297.
Stow, D.A.V., Howell, D.G., Nelson, C.H., 1985. Sedimentary, tectonic and sea-level controls. In: Bouma, A.H., Normark, W.R., Barnes, N.E. (Eds.), Submarine Fans and Related Turbidites Systems. SpringerVerlag, New York, pp. 15–22.
Stow, D.A., Tabrez, A.R., Prins, M.A., 2002. Quaternary sedimentation on the Makran margin: turbidity current–hemipelagic interaction in an active slope–apron system. In: Clift, P.D., Kroon, D., Gaedicke, C., Craig, J. (Eds.), The Tectonic and Climatic Evolution of the Arabian Sea Region: Geol. Soc. Lond. Spec. Publ. , pp. 219–236.
Stuiver, M., Reimer, P.J., Bard, E., Beck, J.W., Burr, G.S., Hughen, K.A., Kromer, B., McCormac, G., van der Plicht, J., Spurk, M., 1998. INTCAL98 Radiocarbon Age Calibration, 24, 000–0 cal BP. Radiocarbon 40 (3), 1041–1083.
Talling, P.J., Amy, L.A., Wynn, R.B., 2007. New insights into the evolution of large-volume turbidity currents: comparison of turbidite shape and previous modelling results. Sedimentology 54, 737–769.
Toucanne, S., Zaragosi, S., Bourillet, J.F., Naughton, F., Cremer, M., Eynaud, F., Dennielou, B., 2008. Activity of the turbidite levees of the Celtic–Armorican margin (Bay of Biscay) during the last 30,000 years: imprints of the last European deglaciation and Heinrich events. Marine Geology 247 (1–2), 84–103.
Tripsanas, E.K., Bryant, W.R., Phaneuf, B.A., 2004. Depositional processes of uniform mud deposits (unifites), Hedberg Basin, northwest Gulf of Mexico: new perspectives. AAPG Bulletin 88 (6), 825–840.
Tripsanas, Efthymios K., Bryant, W.R., Slowey, N.C., Bouma, A.H., Berti, D., 2007. Sedimentological history of Bryant Canyon area, northwest Gulf of Mexico, during the last 135 kyr (Marine Isotope Stages 1–6): a proxy record of Mississippi River discharge. Palaeogeography, Palaeoclimatology, Palaeoecology 246 (1), 137–161.
Underwood, M.B., Moore, G.F., Taira, A., Klaus, A., Wilson, M.E.J., Ferguson, C.L., Hirano, S., Steurer, J., the Leg 190 Shipboard Scientific Party, 2003. Sedimentary and tectonic evolution of a trench–slope basin in the Nankai subduction zone of southwest Japan. Journal of Sedimentary Research 73, 589–602.
Vail, P.R., Mitchum, R.M., 1977. Seismic stratigraphy and global changes of sea-level, Part 1: overview. In: Payton, C.E. (Ed.), Seismic Stratigraphy—Applications to Hydrocarbon Exploration: American Association of Petroleum Geologists Memoir, vol. 26, pp. 2–63.
Van Den Berg Van Saparoea, A.H., Postma, G., 2008. Control of climate change on the yield of river systems. In: Hampson, G.J., Steel, R.J., Burgess, P.M., Darlymple, R.W. (Eds.), Recent Advances in Models of Silliciclastic Shallow-Marine Stratigraphy: SEPM Special Publication, vol. 90.
Vita-Finzi, C., 1987. 14C deformation chronologies in coastal Iran, Greece and Jordan. Journal of the Geological Society, London 144, 553–560.
von Rad, U., Tahir, M., 1997. Late Quaternary sedimentation on the outer Indus shelf and slope (Pakistan): evidence from high-resolution seismic data and coring. Marine Geology 138 (3–4), 193–236.
von Rad, U., Schulz, H., Ali Khan, A., Ansari, M., Berner, U., Cepek, P., Cowie, G., Dietrich, P., Erlenkeuser, H., Geyh, M., Jennerjahn, T., Lückge, A., Marchig, V., Riech, V., Rösch, H., Schaëfer, P., Schulte, S., Sirocko, F., Tahir, M., Weiss, M., 1995. Sampling the oxygen minimum zone off Pakistan: glacial–interglacial variations of anoxia and productivity (preliminary results, SONNE 90 cruise). Marine Geology 125, 7–19.
von Rad, U., Schaaf, M., Michels, K.H., Schulz, H., Berger, W.H., Sirocko, F., 1999a. A 5000-yr record of climate change in varved sediments from the oxygen minimum zone off Pakistan, Northeastern Arabian Sea. Quaternary Research 51 (1), 39–53.
von Rad, U., Schulz, H., Riech, V., den Dulk, M., Berner, U., Sirocko, F., 1999b. Multiple monsoon-controlled breakdown of oxygen-minimum conditions during the past 30,000 years documented in laminated sediments off Pakistan. Palaeogeography, Palaeoclimatology, Palaeoecology 152 (1–2), 129–161.
von Rad, U., Delisle, G., Luckge, A., 2002a. On the formation of laminated sediments on the continental margin off Pakistan. Marine Geology 192 (4), 425–429.
von Rad, U., Khan, A.A., Berger, A., Rammlmair, D., Treppke, U., 2002b. Varves, turbidites and cycles in upper Holocene sediments (Makran slope, northern Arabian Sea). In: Clift, P.D., Kroon, D., Gaedicke, C., Craig, J. (Eds.), The Tectonic and Climatic Evolution of the Arabian Sea Region: Geol. Soc. Lond. Spec. Publ., pp. 387–4706.
Wang, B., Clemens, S.C., Liu, P., 2003. Contrasting the Indian and East Asian monsoons: implications on geologic timescales. Marine Geology 201 (1–3), 5–21.
Wang, P., Clemens, S., Beaufort, L., Braconnot, P., Ganssen, G., Jian, Z., Kershaw, P., Sarnthein, M., 2005. Evolution and variability of the Asian monsoon system: state of the art and outstanding issues. Quaternary Science Reviews 24 (5–6), 595–629.
Weltje, G.J., De Boer, P.L., 1993. Astronomically induced paleoclimatic oscillations reflected in Pliocene turbidite deposits of Corfu (Greece): implications for the interpretation of higher order cyclicity in fossil turbidite systems. Geology 21, 307–310.
White, R.S., Louden, K.E., 1983. The Makran Continental Margin: structure of a thickly sedimented convergent plate boundary. Studies in continental margin geology. In: Watkins, J.S., Drake, C.L. (Eds.), Mem. Am. Ass. Petrol. Geol, vol. 34, pp. 499–518.
Wynn, R.B., Weaver, P.P.E., Masson, D.G., Stow, D.A.V., 2002. Turbidite depositional architecture across three interconnected deep-water basins on the north–west African margin. Sedimentology 49 (4), 669–695.
Zaragosi, S., Bourillet, J.F., Eynaud, F., Toucanne, S., Denhard, B., Van Toer, A., Lanfumey, V., 2006. The impact of the last European deglaciation on the deep-sea turbidite systems of the Celtic–Armorican margin (Bay of Biscay). Geo-Marine Letters 26, 317–329.